

1 **SORORIN is an evolutionary conserved antagonist of WAPL**

2 Ignacio Prusén Mota<sup>1</sup>, Marta Galova<sup>2</sup>, Alexander Schleiffer<sup>2</sup>, Tan-Trung Nguyen<sup>1</sup>, Ines  
3 Kovacikova<sup>1</sup>, Tomoko Nishiyama<sup>2</sup>, Juraj Gregan<sup>1,3,\*</sup>, Jan-Michael Peters<sup>2,\*</sup> and Peter  
4 Schlögelhofer<sup>1,\*</sup>

5

6 1 Department of Chromosome Biology, Max Perutz Labs, University of Vienna, Vienna  
7 Biocenter (VBC), Vienna, Austria

8 2 Research Institute of Molecular Pathology (IMP), Vienna Biocenter (VBC), Vienna,  
9 Austria

10 3 Department of Applied Genetics and Cell Biology, Institute of Microbial Genetics,  
11 University of Natural Resources and Life Sciences, Tulln an der Donau, Austria

12

13 \* Correspondence to:

14 Peter Schlögelhofer – [peter.schloegelhofer@univie.ac.at](mailto:peter.schloegelhofer@univie.ac.at);

15 Jan-Michael Peters – [Jan-Michael.Peters@imp.ac.at](mailto:Jan-Michael.Peters@imp.ac.at);

16 Juraj Gregan – [juraj.gregan@univie.ac.at](mailto:juraj.gregan@univie.ac.at)

17 **Abstract**

18 Cohesin mediates sister chromatid cohesion to enable chromosome segregation and  
19 DNA damage repair. To perform these functions, cohesin needs to be protected from  
20 WAPL, which otherwise releases cohesin from DNA. It has been proposed that cohesin  
21 is protected from WAPL by SORORIN. However, *in vivo* evidence for this antagonism  
22 is missing and SORORIN is only known to exist in vertebrates and insects. It is  
23 therefore unknown how important and widespread SORORIN's functions are. Here we  
24 report the identification of SORORIN orthologs in *Schizosaccharomyces pombe* (Sor1)  
25 and *Arabidopsis thaliana* (AtSORORIN). *sor1*Δ mutants display cohesion defects,  
26 which are partially alleviated by *wpl1*Δ. *Atsororin* mutant plants display dwarfism,  
27 tissue specific cohesion defects and chromosome mis-segregation. Furthermore,  
28 *Atsororin* mutant plants are sterile and separate sister chromatids prematurely at  
29 anaphase I. The somatic, but not the meiotic deficiencies can be alleviated by loss of  
30 WAPL. These results provide *in vivo* evidence for SORORIN antagonizing WAPL,  
31 reveal that SORORIN is present in organisms beyond the animal kingdom and indicate  
32 that it has acquired tissue specific functions in plants.

## 33 **Introduction**

34 Eukaryotic cells perform a complex series of events in order to equally distribute the  
35 replicated genome among their daughter cells. DNA replication is not immediately  
36 followed by karyokinesis and the newly formed sister chromatids are physically linked  
37 for long periods of time until their disjunction during mitosis or meiosis <sup>1,2</sup>. Sister  
38 chromatid cohesion (SCC) is mediated by the cohesin complex, which is thought to  
39 topologically entrap DNA helices from both newly replicated sisters <sup>3,4</sup>. While SCC  
40 promotes chromosome biorientation and DNA damage repair, cohesin can also extrude  
41 loops of DNA and facilitate distant intra-chromatid interactions, supporting further roles  
42 in chromatin organization and gene expression <sup>5</sup>.

43 Cohesin's core subunits have been identified and characterized in all branches of the  
44 eukaryotic kingdom including yeast and plants <sup>6,7</sup>. As a member of the Structural  
45 Maintenance of Chromosome (SMC) protein family, cohesin is formed by a  
46 heterodimer of SMC1 and SMC3. These proteins fold back on themselves at the hinge  
47 domain, where they interact with each other, to form long antiparallel coiled-coil  
48 structures. At the other end, their ATPase head domains are bridged together by an  $\alpha$ -  
49 kleisin subunit, RAD21 (also known as Scc1 or Mcd1) or its meiotic counterparts REC8  
50 and RAD21L <sup>8-10</sup>. These heterotrimeric ring-like structures crucially depend on the  
51 recruitment of SCC3 (SA or STAG proteins) to fulfil their chromatin-related functions.  
52 SCC3 contributes to cohesin loading, maintenance on chromosomes and its subsequent  
53 release from DNA <sup>11-16</sup>. Together, these four proteins form the cohesin core complex.

54 In addition to SCC3, two further HAWK proteins (HEAT repeat proteins Associated  
55 With Kleisin), SCC2 (also known as NIPBL or Mis4) and PDS5 <sup>17</sup>, bind to kleisin in a  
56 mutually exclusive manner to regulate cohesin behaviour <sup>18,19</sup>. SCC2 is needed to  
57 stimulate cohesin's ATPase activity <sup>16,18,20,21</sup> and has been proposed to load cohesin  
58 onto DNA <sup>11,22</sup>. *In vitro* experiments have shown that NIPBL is further required for  
59 cohesin-mediated loop extrusion <sup>20,21</sup>. PDS5 and WAPL can disrupt the interaction  
60 between the SMC3 and kleisin subunits, thereby releasing cohesin from chromatin <sup>23-26</sup>.  
61 While cohesin shows a highly dynamic behaviour through cycles of association and  
62 release from chromatin, especially during G1, a fraction of cohesin becomes stably  
63 bound to DNA after replication and mediates SCC <sup>27,28</sup>. Establishment of cohesion  
64 during DNA replication requires acetylation of two lysine residues on SMC3 by the

65 conserved acetyltransferase Eco1/CTF7<sup>29–33</sup>. In yeast, Pds5 is required for the  
66 acetylation process and for stabilizing cohesin on chromatin<sup>25</sup>. Inactivation of cohesin  
67 loading during G1 induces complete cohesin dissociation from DNA in a Wpl1-  
68 dependent manner, whereas if inactivation takes place during G2, some cohesin remains  
69 chromatin-bound<sup>28</sup>. In *A. thaliana*, mutation of four of the five *PDS5* genes leads to  
70 mild defects in meiosis and to severe deficiencies in development, fertility and somatic  
71 homologous recombination (HR)<sup>34</sup>. Inactivation of both copies of *WAPL* in *A. thaliana*  
72 only mildly affects overall plant development and fertility<sup>35</sup>, but rescues the dramatic  
73 somatic deficiencies associated with loss of CTF7<sup>36,37</sup>.

74 In vertebrates and *Drosophila*, an additional protein factor, Sororin, is recruited to the  
75 cohesin complex in a replication and SMC3-acetylation dependent manner<sup>38–43</sup>. Sororin  
76 promotes SCC until the onset of anaphase by displacing WAPL from PDS5 and  
77 counteracting its releasing effects<sup>40</sup>. Both WAPL and Sororin bind to PDS5 through  
78 conserved FGF and YSR motifs<sup>40,44</sup>.

79 In somatic cells, Sororin accumulates on chromatin between S and G2 phases and  
80 becomes dispersed in the cytoplasm after nuclear envelope breakdown except at  
81 centromeric regions where it persists until metaphase<sup>40,42</sup>, consistent with its function in  
82 promoting SCC<sup>43,45</sup>. This suggests that Sororin, as the cohesin complex, is removed  
83 from chromosomes in a stepwise manner<sup>46</sup>. First, the so-called prophase pathway  
84 removes chromosomal arm cohesin in a non-proteolytic manner during the first stages  
85 of mitosis and meiosis. This process largely depends on WAPL and phosphorylation of  
86 STAG2<sup>13,23,47,48</sup>. Sororin phosphorylation has been proposed to participate in both  
87 processes: Cdk1-phosphorylated Sororin may act as a docking protein and recruit Polo-  
88 like kinase 1 (Plk1) to mediate STAG2 phosphorylation<sup>49</sup>. Besides, Aurora B and Cdk1  
89 phosphorylate Sororin on several sites and destabilise its association with PDS5,  
90 thereby promoting WAPL-mediated removal of cohesion<sup>50,51</sup>. At centromeres, the  
91 Shugoshin-PP2A complex protects cohesin from the prophase pathway by keeping  
92 Sororin and cohesin subunits in a dephosphorylated state<sup>51–53</sup>. During the metaphase-to-  
93 anaphase transition, the anaphase-promoting complex/cyclosome (APC/C<sup>Cdc20</sup>) targets  
94 phosphorylated Securin for degradation to promote the separase-mediated cleavage of  
95 the phosphorylated kleisin subunit<sup>42,54–56</sup>.

96 Current data suggest that the main function of Sororin is to counteract the activity of  
97 WAPL. While WAPL appears conserved across kingdoms, including yeasts and land

98 plants, no conserved WAPL antagonist has been described so far. SMC3 acetylation has  
99 been proposed to be sufficient to counteract the function of WAPL in organisms thought  
100 to lack Sororin, like yeast and plants<sup>37,57</sup>. In *Drosophila melanogaster*, the Sororin-  
101 related protein Dalmatian has been characterized<sup>40</sup>. Dalmatian combines protein  
102 functions of Sororin and Shugoshin to promote and protect cohesion<sup>41</sup>. Recently, a  
103 meiosis I-specific WAPL antagonist (SWI1), that shares no sequence homology to  
104 Sororin, has been characterized in *A. thaliana*<sup>58</sup>.

105 To identify possible homologs of *Sororin* we performed a thorough bioinformatics  
106 analysis. Our searches revealed putative Sororin relatives in various lower and higher  
107 eukaryotes. Here we show that *S. pombe* Sor1 is required for efficient sister chromatid  
108 cohesion and that *wpl1* deletion partially suppresses defects caused by the *sor1Δ*  
109 mutation. We also demonstrate that Sor1 physically interacts with the cohesin subunit  
110 Psm3 (SMC3) and Pds5. We furthermore show, that the *A. thaliana* *Sororin* homologue  
111 (*AtSORORIN*) is essential for vegetative development and microsporogenesis. Lack of  
112 *AtSORORIN* leads to tissue specific reduction or loss of SCC and chromosomal mis-  
113 segregation. Consistent with *AtSORORIN*'s proposed function, these somatic  
114 phenotypes can be alleviated by loss of WAPL. *Atsororin* mutant plants are sterile,  
115 affected in male meiosis with chromatids displaying premature loss of cohesion and  
116 splitting of sister-centromeres at anaphase I. Interestingly, the meiotic defects cannot be  
117 alleviated by loss of WAPL. Taken together, we provide the first organismal *in vivo*  
118 evidence for Sororin antagonizing WAPL function and demonstrate that Sororin is an  
119 evolutionary conserved cohesin regulator that has acquired additional functions in  
120 plants.

121

122

## 123 **Results**

### 124 ***S. pombe* Sor1 and *A. thaliana* AtSORORIN share sequence similarities with** 125 **metazoan Sororin proteins**

126 To identify possible orthologs of *Sororin*, we performed a comprehensive  
127 bioinformatics analysis using sensitive remote homology searches. Our searches  
128 revealed putative Sororin proteins in both lower and higher eukaryotes including  
129 various yeast and plant species. They all show only weak overall sequence conservation  
130 with their vertebrate counterparts but they share various characteristic features. The *S.*  
131 *pombe* (SPAC9E9.05) and the *A. thaliana* (At3g56250) gene candidates which both  
132 encode short proteins were analyzed in detail. Vertebrate Sororin and Wapl proteins  
133 interact with Pds5 through their YSR and FGF motifs<sup>40,44</sup>. Whereas SPAC9E9.05 has a  
134 putative FGF motif, such sequence is not present in the plant candidate. A KEN box  
135 targets vertebrate Sororin and *Drosophila* Dalmatian for APC/C<sup>Cdh1</sup>-dependent  
136 degradation, but has not been found in either the plant (At3g56250) or the yeast  
137 (SPAC9E9.05) candidates. Similar to metazoan Sororin, the proteins encoded by  
138 SPAC9E9.05 and At3g56250 have a conserved motif, referred to as the Sororin domain,  
139 preceded by a K/R-rich domain at their C-termini (Figure 1a). The Sororin domain has  
140 been implicated in interactions with STAG2 and contains two conserved phenylalanine  
141 residues important for the maintenance of sister chromatid cohesion (Figure 1b)<sup>59,60</sup>.

142 The *S. pombe* Sororin candidate, SPAC9E9.05, has so far been annotated as a poorly  
143 characterized *Schizosaccharomyces* specific protein<sup>61</sup>. Interestingly, a *SPAC9E9.05*  
144 deletion mutant was identified in a screen for mutants that showed negative synthetic  
145 growth interaction with the cohesion-defective mutants *eso1-G799D* (Eso1 is the *S.*  
146 *pombe* ortholog of Escol1/2 and CTF7<sup>62</sup>) and *mis4-242* (Mis4 is the *S. pombe* ortholog  
147 of NIPBL<sup>63</sup>), suggesting that *SPAC9E9.05* may be involved in regulation of sister  
148 chromatid cohesion<sup>64</sup>. Given the similarity of *S. pombe* SPAC9E9.05 and *Arabidopsis*  
149 At3G56250 with metazoan Sororin and the data presented below, we decided to name  
150 their encoding genes *sor1* (*Sororin-like 1*) and *AtSORORIN*, respectively.

### 151 ***S. pombe* Sor1 is a nuclear protein involved in sister chromatid cohesion**

152 If *S. pombe* Sor1 was functionally related to mammalian Sororin, then it should be  
153 present in the nucleus. Nuclear localization of Sor1 was previously observed when  
154 expressed under the control of a strong *nmt1* promoter<sup>65</sup>. To analyze Sor1 localization,

155 we expressed Sor1-GFP from its native promoter. In an asynchronously growing  
156 culture, Sor1-GFP localized to the nucleus in most cells (Supplementary Figure 1a).  
157 Immunostaining experiments confirmed the nuclear localization of Sor1-Flag during all  
158 tested cell cycle stages (Supplementary Figure 1b).

159 To assess the role of Sor1 in regulation of cohesion, we analyzed sister chromatid  
160 cohesion at the centromeric region (*cen2*-GFP) of chromosome 2. In metaphase, *sor1Δ*  
161 mutant cells showed a small, but significant, increase of split sister centromeres (Figure  
162 2a), indicative of a cohesion defect between sister centromeres. However, the role of  
163 Sor1 in sister chromatid cohesion is not essential because we observed no defects in  
164 chromosome segregation in *sor1Δ* cells (Figure 2b). In mammalian cells, Sororin is  
165 dispensable for sister chromatid cohesion in the absence of WAPL<sup>40</sup>. We therefore  
166 analyzed sister chromatid cohesion in cells lacking Wpl1, the fission yeast ortholog of  
167 WAPL<sup>62</sup>. Interestingly, the increase in split sister centromeres in *sor1Δ* mutant cells  
168 was prevented in *sor1Δ wpl1Δ* double mutants (compared to wild type), suggesting that  
169 similarly to mammalian cells *wpl1* deletion reduces the sister chromatid cohesion defect  
170 caused by the *sor1Δ* mutation (Figure 2a).

171 Deletion of *sor1* showed negative synthetic growth interaction with both *esol-G799D*  
172 and *mis4-242* mutations but the cause of these defects is unknown<sup>64</sup>. We asked whether  
173 defective segregation of chromosomes contributes to this growth defect. Indeed, we  
174 observed a higher frequency of lagging chromosomes associated with a higher rate of  
175 chromosome mis-segregation in *esol-G799D sor1Δ* and *mis4-242 sor1Δ* double  
176 mutants as compared to single mutants (Figure 2b). This observation is consistent with  
177 the role of Sor1 in sister chromatid cohesion regulation.

178 In telophase and G1, mammalian Sororin is targeted by APC/C for degradation<sup>42</sup>. We  
179 therefore tested whether the fission yeast Sor1 is an APC/C substrate, despite the lack of  
180 a defined KEN box. We added *in vitro* translated Sor1-HA to interphase *Xenopus* egg  
181 extracts in the presence of cycloheximide followed by addition of Cdh1 to activate  
182 APC/C<sup>Cdh1</sup>. We also added *in vitro* translated Sor1-HA to meiotic metaphase-arrested  
183 CSF extracts in the presence of cycloheximide followed by addition of CaCl<sub>2</sub> to activate  
184 APC/C<sup>Cdc20</sup>. As expected, activation of APC/C<sup>Cdc20</sup> led to a rapid degradation of the  
185 APC/C<sup>Cdc20</sup> substrate Cyclin B2 and also endogenous *Xenopus* Sororin was degraded  
186 within few minutes after activation of APC/C<sup>Cdh1</sup>. However, we did not observe

187 degradation of *S. pombe* Sor1 by either APC/C<sup>Cdh1</sup> or APC/C<sup>Cdc20</sup> (Supplementary  
188 Figure 1c).

189 **Conserved residues in the Sororin domain are important for Sor1 function and**  
190 **association with cohesin**

191 Mammalian Sororin physically interacts with cohesin and Pds5 and these interactions  
192 are essential for Sororin's function<sup>40,59,60</sup>. If the fission yeast Sor1 was an ortholog of  
193 metazoan Sororin, Sor1 should interact with cohesin and/or Pds5. We indeed observed  
194 that Pds5-Myc co-immunoprecipitated with Sor1-Pk and Sor1-Pk co-  
195 immunoprecipitated with Psm3-GFP (Figure 2c, d).

196 The Sororin domain is required for sister chromatid cohesion and association of Sororin  
197 with cohesin in mammalian cells<sup>59,60</sup>. To test whether the Sororin domain of *S. pombe*  
198 Sor1 is important for its association with cohesin in fission yeast, we analyzed the  
199 ability of Psm3-GFP to immunoprecipitate mutant protein Sor1-D303A-Pk, in which a  
200 conserved aspartic acid residue D303 in the Sororin domain has been replaced by  
201 alanine. Sor1-D303A-Pk co-immunoprecipitated less efficiently with the Psm3-GFP  
202 protein, compared to wild type Sor1-Pk, suggesting that the conserved residue D303 in  
203 the Sororin domain of Sor1 is important for the association of Sor1 with cohesin (Figure  
204 2d).

205 We then asked whether the interaction between *S. pombe* Sor1 and cohesin is  
206 functionally relevant. As expected, expression of a wild type Sor1 rescued the growth  
207 defect of the *eso1-G799D sor1Δ* double mutant to the level of the *eso1-G799D* single  
208 mutant. However, expression of the Sor1-D303A mutant, which weakens the interaction  
209 between Sor1 and cohesin, did not restore the growth defect of *eso1-G799D sor1Δ*  
210 double mutants (Figure 2e). Mutating three other conserved residues in the Sororin  
211 domain of Sor1 (F299A, V302A and Y305A) resulted in a similar phenotype (Figure  
212 2e). The observed mutant phenotype was not due to lack of Sor1 expression as all four  
213 Sor1 mutant proteins (Sor1-D303A-TAP, Sor1-F299A-TAP, Sor1-V302A-TAP and  
214 Sor1-Y305A-TAP) were expressed, although at reduced levels (Supplementary Figure  
215 1d).

216 Taken together, we show that fission yeast Sor1 shares similarity with metazoan Sororin  
217 proteins. Sor1 is associated with the cohesin complex and *sor1Δ* mutant cells show  
218 defects consistent with the role of Sor1 in regulation of sister chromatid cohesion.



219 Conserved residues at the C-terminus of Sor1 are important for the Sor1 function and its  
220 association with cohesin. Unlike metazoan Sororin proteins, Sor1 is not essential for  
221 sister chromatid cohesion, suggesting that fission yeast possesses mechanisms that are  
222 able to compensate for the absence of Sor1. Our results are consistent with the notion  
223 that Sor1 is an ortholog of Sororin in the fission yeast *S. pombe*.

## 224 *A. thaliana* **SORORIN** is essential for vegetative development and 225 **microsporogenesis**

226 Our findings obtained in *S. pombe* motivated us to analyze a Sororin candidate in a non-  
227 vertebrate higher eukaryote. The *A. thaliana* *SORORIN* gene candidate (At3g56250)  
228 consists of four exons and codes for a relatively small protein (222 amino acids). Using  
229 CRISPR-Cas9 technology we generated a 5 bp deletion in its first exon, creating a  
230 premature stop codon (Figure 3a). Heterozygous *Atsororin* +/- plants appear like wild  
231 type with only minimally reduced seed numbers, but homozygous mutants display a  
232 prominent dwarf phenotype, have few and short siliques and epinastic rosette leaves  
233 with short petioles that grow around an undersized stem (Figure 3b). This dramatic  
234 phenotype can be complemented with a transgene containing the wild-type gene,  
235 including all up- and down-stream regulatory sequences and introns (Supplementary  
236 Figure 2a, b), corroborating that the mutation in the *AtSORORIN* gene indeed caused the  
237 observed aberrations. Plant roots and shoots develop from meristems, which are formed  
238 by actively dividing cells that self-renew and differentiate into new tissue. Root  
239 development is severely affected by the lack of *AtSORORIN*. *Atsororin* mutant plant  
240 roots grow significantly shorter than those of wild type, and they completely lose the  
241 characteristic layered cellular organization (Figure 3c, d). Moreover, mutant plants are  
242 sterile since their short siliques do not develop viable seeds (Figure 3e).

243 Heterozygous, self-pollinated *Atsororin* +/- plants have less than 4% homozygous  
244 *Atsororin* -/- offspring, representing a significant deviation from the expected  
245 Mendelian segregation ratio (Figure 3f). Reciprocal crosses between *Atsororin* +/-  
246 heterozygous mutant plants and wild type plants revealed that the distortion of  
247 segregation ratios is exclusively caused by the male generative cells (Figure 3g). In fact,  
248 the morphology of *Atsororin* mutant anthers is abnormal, their size decreased and the  
249 amount of shed pollen strongly reduced. A test for pollen viability (Alexander staining)  
250 showed that unlike wild-type plants, *Atsororin* mutants produce only very few pollen  
251 grains of which only very few are viable (Figure 3h).

## 252 **Loss of WAPL rescues *Atsororin*-associated defects**

253 In mammalian cells, Sororin is needed to counteract the cohesin-releasing activity of  
254 Wapl, and therefore deficiencies related to loss of Sororin can be suppressed by loss of  
255 Wapl<sup>40</sup>. Arabidopsis *wapl1-1 wapl2* double mutants exhibit normal vegetative growth  
256 and only a mild reduction in fertility (Figure 3b)<sup>35</sup>. The *Atsororin*-associated somatic  
257 defects can be suppressed by the *wapl1-1 wapl2* double mutant, underlining that  
258 Arabidopsis *SORORIN* is a *bona-fide* relative of its vertebrate counterpart. In the  
259 *Atsororin wapl1-1 wapl2* triple mutant normal growth of the aerial plant parts and of the  
260 roots is restored (Figure 3b-d).

261 WAPL inactivation only leads to a limited rescue of the fertility defect observed in  
262 *Atsororin* mutants. *Atsororin wapl1-1 wapl2* anthers are nearly as small as those of  
263 *Atsororin* single mutants and only very few viable pollen grains are formed (Figure 3h).  
264 Correspondingly, the triple mutant produces only very few seeds, but still significantly  
265 more than the *Atsororin* single mutant (wild type  $55 \pm 4$  seeds/silique (n=74), *wapl1-1*  
266 *wapl2*  $36 \pm 9$  seeds/silique (n=144; p<0.0001), *Atsororin*  $0.096 \pm 0.35$  seeds/silique  
267 (n=52; p<0.0001); *Atsororin wapl1-1 wapl2*  $5 \pm 4$  seeds/silique (n=166; p<0.0001)  
268 (Figure 3e).

## 269 **AtSORORIN is essential in a sub-set of tissues**

270 The data, especially the epistatic relation to *WAPL*, suggested that the gene product of  
271 *AtSORORIN* acts in a similar manner as its vertebrate counterpart. We anticipated that  
272 the most obvious molecular phenotype of *Atsororin* mutants should be pre-mature loss  
273 of sister-chromatid cohesion. To analyze chromosome numbers and sister chromatid  
274 cohesion we prepared mitotic cell nuclei samples and specifically stained centromeres  
275 (via fluorescent *in situ* hybridization, FISH).

276 Indeed, interphase nuclei from roots of *Atsororin* mutant plants contain on average  
277  $16.82 \pm 3.68$  centromere signals (n=34). This is significantly more compared to wild  
278 type ( $10.02 \pm 0.1458$  centromere signals; n=93; p<0.0001), *wapl1-1 wapl2* double  
279 mutants ( $10.32 \pm 1.66$  centromere signals; n=73; p<0.0001) and *Atsororin wapl1-1*  
280 *wapl2* triple mutants ( $10.49 \pm 1.83$  centromere signals; n=59; p<0.0001) (Figure 4a, b).  
281 We attribute the severe mis-organisation of cells in the *Atsororin* mutant roots (Figure  
282 3c) (Supplementary movies 1 – 4) and the arbitrary chromosome numbers in interphase  
283 nuclei to massive chromosome mis-segregation due to pre-mature loss of cohesin. Since

284 the homozygous *Atsororin* mutant plants are under-represented and the mutant root  
285 material is scarce and experimentally difficult to process we could only obtain a few  
286 cells at metaphase. While in wild-type 10 doublet signals can be seen, in *Atsororin*  
287 plants individual chromatids are arranged at the metaphase plate. The anticipated pre-  
288 mature loss of SCC leads to random segregation of chromatids during anaphase in  
289 *Atsororin* mutants. Importantly, *Atsororin wapl1-1 wapl2* triple mutants are much less  
290 affected than the *Atsororin* single mutant (Figure 3c; Figure 4a, b).

291 Somatic interphase cell nuclei isolated from leaves of *Atsororin* mutant plants, had a  
292 close to regular number of chromosomes ( $10,3 \pm 0,5746$  centromere signals; n=53),  
293 which is still significantly different when compared to wild-type plants (10 centromere  
294 signals; n=84;  $p < 0.0001$ ), *wapl1-1 wapl2* double mutants (10 centromere signals; n=68;  
295  $p < 0.0001$ ) or *Atsororin wapl1-1 wapl2* triple mutants (10 centromere signals; n=82;  
296  $p < 0.0001$ ) (Supplementary Figure 2c, d).

297 We also prepared somatic cells from inflorescences, containing a large number of  
298 actively dividing cells that can be readily processed and analyzed (Figure 4c). As for the  
299 leaf cells, we established first the number centromeric signals of interphase nuclei. We  
300 found, similar to the numbers obtained from leaf cells and in contrast to the ones  
301 obtained from root cells, that most cells contain the correct number of chromosomes in  
302 *Atsororin* mutants ( $10.26 \pm 1.25$  centromere signals; n=266) but still significantly  
303 different when compared to wild type (10 centromere signals; n=224;  $p < 0.0001$ ),  
304 *wapl1-1 wapl2* double mutants ( $10.01$  centromere  $\pm 0.09$  centromere signals; n=238;  
305  $p < 0.0001$ ) or *Atsororin wapl1-1 wapl2* triple mutants ( $10.09$  centromere signals; n=236;  
306  $p < 0.0001$ ) (Figure 4d).

307 Since a large number of actively dividing cells in anaphase could be observed in the  
308 inflorescence tissue we were also in the position to monitor chromosome segregation.  
309 In accordance with the mild aberrations of chromosome numbers in interface nuclei, we  
310 observed mostly regular chromosome disjunction in *Atsororin* nuclei from  
311 inflorescences (97% symmetric disjunction, n=133) with 10 separating chromosomes at  
312 either side of the division plane. Those *Atsororin* plants (13/133) that carried 11  
313 chromosomes in all cells, most likely obtained via a gamete with a supernumerary  
314 chromosome, showed regular disjunction. In this sense, the occurrence of symmetric  
315 divisions was not significantly different from wild-type plants (n=112,  $p = 0.2525$ ) and  
316 *wapl1-2 wapl2* (n=119,  $p = 0.9999$ ) and *Atsororin wapl1-2 wapl2* (n=118,  $p = 0.6246$ )

317 mutants.

318 We also measured the inter-sister centromere distance during prophase and  
319 prometaphase (Figure 4c, e, f) in somatic cells from inflorescences. Post S-phase 10  
320 doublet signals can be seen in all genotypes tested. While the mutation in *AtSORORIN*  
321 does not lead to complete loss of cohesion between sister chromatids, the distance  
322 between the 10 centromeric doublet signals is significantly increased compared to wild  
323 type (Prophase: 457.6 nm in *Atsororin*, n=39; 378.9 nm in wild type, n=45; p<0.0001.  
324 Prometaphase: 699 nm in *Atsororin*, n=55; 562.9 nm in wild type, n=42; p<0.0001).  
325 The sister-centromere distance is, as anticipated, significantly shortened in *wapl1-2*  
326 *wapl2* mutants compared to wild type (Prophase: 294.2 nm in *wapl1-2 wapl2*, n=37;  
327 p<0.0001. Prometaphase: 481.4 nm in *wapl1-2 wapl2*, n=43; p<0.01). During prophase,  
328 the *Atsororin wapl1-2 wapl2* triple mutants have a centromeric distance that is not  
329 different from wild type (349.2 nm, n=50; p=0.2695), significantly shorter than the  
330 *Atsororin* single mutant (457.6 nm, p<0.0001) and increased when compared to *wapl1-2*  
331 *wapl2* mutants (294.2 nm, p<0.0001). At prometaphase the centromeric distance of  
332 *Atsororin wapl1-2 wapl2* is as tight as in the *wapl1-2 wapl2* mutant (446.1 nm in  
333 *Atsororin wapl1-2 wapl2*, n=49; p=0.4004). It is interesting to note that in *wapl1-2*  
334 *wapl2* double mutants, cohesion of sister chromatid arms is maintained in prometaphase  
335 since no individual arms can be distinguished. This also holds true in the *Atsororin*  
336 *wapl1-2 wapl2* triple mutant background.

337 Taken together, we conclude that both AtSORORIN and WAPL impact sister-  
338 chromatid cohesion, and that AtSORORIN is not the exclusive antagonist of WAPL  
339 activity in all somatic plant tissues.

### 340 **AtSORORIN is needed for centromeric sister chromatid cohesion during male** 341 **meiosis**

342 Our analysis indicated that somatic divisions in root cells and microsporogenesis are  
343 most severely affected by loss of *AtSORORIN*. To analyze if the underlying cause for  
344 the latter can be related to a perturbation of male meiosis we prepared chromosome  
345 spreads from meiocytes. Comparing wild-type and *Atsororin* meiocytes it is apparent  
346 that AtSORORIN is not an essential factor for sister chromatid cohesion in prophase I.  
347 Meiocytes from *Atsororin* plants show normal chromosome condensation and pairing  
348 during pachytene and also chiasmata at diakinesis. Bivalents were properly orientated at

349 the metaphase I plate. Yet, in anaphase I sister chromatids split pre-maturely and were  
350 subsequently segregated at random in meiosis II (Figure 5). While in anaphase I /  
351 telophase I we observed 5 DAPI-stained bodies at each pole of the dyad in wild type, in  
352 *Atsororin* mutants around 10 DAPI stained bodies can be seen. In metaphase II these 10  
353 DAPI stained bodies could not be aligned properly, were distributed at random during  
354 anaphase II and subsequently led to unbalanced tetrads. Supernumerary DAPI stained  
355 bodies, which we interpret as individual chromatids, were detected in 71% of *Atsororin*  
356 meiocytes during prophase II-metaphase II stages (n=38), while this was never observed  
357 in wild type (n=67; p<0.0001).

358 The *wapl1-2 wapl2* double mutants showed strengthened cohesion, characterized by the  
359 distinct shape of bivalents at metaphase I, as previously described<sup>35</sup>, and regular  
360 distribution of chromosomes at meiosis I (n=32) and II. Importantly, in male meiocytes  
361 of *Atsororin wapl1-2 wapl2* triple mutants, premature loss of sister chromatids persists.  
362 Supernumerary chromatids were observed in 80% of all anaphase I / telophase I  
363 meiocytes in the triple mutant (n=40; p<0.0001 compared to wild-type or *wapl1-2*  
364 *wapl2*). This means, that the premature loss of centromeric sister chromatid cohesion at  
365 anaphase I / telophase I in *Atsororin* mutants cannot be rescued by loss of WAPL.

366 To determine the precise timing of loss of sister chromatid cohesion during meiosis of  
367 *Atsororin* mutant plants we performed centromeric FISH analysis on meiotic spreads  
368 (Figure 6a). As mentioned above, homologous chromosome pairing appeared normal in  
369 *Atsororin* mutants, underlined by the presence of 5 dominant CEN signals observed at  
370 pachytene stage. During late metaphase I/early anaphase I, five pairs of CEN signals  
371 were observed in wild type, with two distinct signals per bivalent (each signal  
372 representing two fused sister centromeres) that were orientated to opposite poles. In  
373 *Atsororin* mutants, homologous chromosomes showed proper bipolar orientation at  
374 metaphase I but the centromeric signals pointing to either pole were often split. All of  
375 the observed *Atsororin* metaphases had more than 10 CEN signals (n=24), indicating  
376 that sister chromatid centromeres were not fused as in wild type (Figure 6a, b). We  
377 quantified the number of centromeric signals observed at metaphase I (including cells  
378 from metaphase I to prophase II stages) and metaphase II stages in wild-type plants and  
379 *Atsororin*, *wapl1-2 wapl2* double and *Atsororin wapl1-2 wapl2* triple mutants (Figure  
380 6c, d). While meiocytes from wild-type and *wapl1-2 wapl2* mutant plants did mostly  
381 not suffer from premature splitting of sister-centromeres at metaphase I (93.4% and

382 91.3% of cells with 10 centromere signals respectively, n=76 in wild type, n=23 in  
383 *wapl1-2 wapl2*; p=0.6622) and had perfectly paired sister-centromeres at metaphase II  
384 (n=17 in wild type, n=10 in *wapl1-2 wapl2*), *Atsororin* and *Atsororin wapl1-2 wapl2*  
385 mutants displayed split sister-centromere signals at metaphase I (n=24, p<0.0001 in  
386 *Atsororin*; n=31, p<0.0001 in the triple mutant), and non-paired sister-centromeres at  
387 metaphase II (n=13, p<0.0001 in *Atsororin*; n=17, p<0.0001 in *Atsororin wapl1-2*  
388 *wapl2* mutants).

389 As mentioned above, after loss of sister chromatid cohesion, progression through  
390 meiosis II is compromised and in *Atsororin* and *Atsororin wapl1-2 wapl2* mutants  
391 individual chromatids segregated at random. We quantified tetrads with balanced  
392 chromosome numbers (Figure 6e). While in wild-type plants, all meiocytes generated  
393 balanced tetrads (n=33), none of the *Atsororin* mutants produced balanced tetrads  
394 (n=25; p<0.0001), *wapl1-2 wapl2* mutants produced 75% of balanced tetrads (n=28;  
395 p<0.01) and *Atsororin wapl1-2 wapl2* none (n=18; p<0.0001). These observations lend  
396 further support to the notion that the meiotic deficiencies in AtSORORIN cannot be  
397 rescued by loss of WAPL.

398 It is interesting to note that while univalent chromosomes were not observed in WT or  
399 *wapl1-1 wapl2* mutants, a significant fraction (13%) of *Atsororin* meiocytes showed  
400 presence of an extra univalent chromosome (scored at diakinesis-metaphase I stages;  
401 n=53; p<0.01). Presence of extra chromosomes could be the consequence of a previous  
402 non-disjunction event in the meiocyte precursor cells, or the result of fertilization  
403 between unbalanced generative cells (see also above). Interestingly, we did not observe  
404 univalents in the *Atsororin wapl1-1 wapl2* triple mutants (n=32).

#### 405 **AtSORORIN does not affect meiotic cohesin abundance and axis formation in** 406 **meiotic prophase**

407 We were curious to understand AtSORORIN's impact on cohesin abundance in a  
408 severely affected tissue. We therefore performed chromosome spreads of male  
409 meiocytes and subsequent immune-staining using antibodies directed against the  
410 cohesin subunit SCC3 and the meiosis specific kleisin subunit REC8 (Figure 7;  
411 Supplementary Figure 3). We scored cells at the zygotene/pachytene transition as  
412 cohesins can still be observed well at this stage. To correctly stage progression of  
413 meiosis, we also detected the meiotic axis component ASY1 and the transverse filament

414 protein of the synaptonemal complex (SC), ZYP1. Our analysis shows that during  
415 meiotic prophase, axis formation, as judged from the ASY1 signal, and SC formation,  
416 as judged from the ZYP1 signal, is indistinguishable from wild type in *Atsororin*,  
417 *wapl1-2 wapl2* and *Atsororin wapl1-2 wapl2* mutants. Furthermore, cohesion  
418 abundance and deposition, as judged from the SCC3 and REC8 signals, along the  
419 chromosome arms appears unaffected in *Atsororin*, *wapl1-2 wapl2* and *Atsororin*  
420 *wapl1-2 wapl2* mutants (Figure 7; Supplementary Figure 3).

## 421 Discussion

422 Cohesin complexes are evolutionarily ancient inventions of nature, involved in proper  
423 chromosome disjunction in mitosis and meiosis, but also essential for chromosome  
424 organization<sup>66</sup>. In animal cells, Wapl has been recognized as a cohesin removal factor  
425 which itself is kept in check by the antagonizing protein Sororin<sup>23,40,45</sup>. While cohesin  
426 complex proteins, Wapl and Eco1-dependent acetylation of cohesin are conserved from  
427 yeast and plants to humans, Sororin was thought to be present only in metazoans<sup>5,41</sup>. A  
428 Sororin-like protein has been characterized in the fly, with a peculiar dual function; it  
429 serves as a Wapl antagonist and also as a centromeric cohesion protector<sup>40,41</sup>. In  
430 *Arabidopsis*, the protein SWI1 antagonizes the function of WAPL, but exclusively only  
431 during meiotic prophase I, and it shares no sequence homology with the vertebrate or  
432 fly relatives<sup>58,67</sup>. These results suggested that WAPL antagonists should also be present  
433 in the genomes of other eukaryotes, but possibly strongly diverged in sequence or  
434 occurring as functional domain in the context of larger proteins.

435 Applying sensitive remote homology searches, we identified putative Sororin relatives  
436 in various organisms, including *S. pombe* and *A. thaliana*, which are separated by  
437 approximately 1.5 billion years of independent development.

438 We show that Sor1, the *S. pombe* Sororin-relative, physically interacts with cohesin (via  
439 SMC3/Psm3) and Pds5. However, we observed only a mild sister chromatid cohesion  
440 defect in *sor1Δ* cells, suggesting that there are other mechanisms that compensate for  
441 the absence of Sor1. Importantly, *wpl1* deletion partially suppressed the sister chromatid  
442 cohesion defect caused by the *sor1Δ* mutation, suggesting that, similarly as metazoan  
443 Sororin, Sor1 antagonizes the function of Wapl. Our results are consistent with the  
444 notion that Sor1 is an ortholog of Sororin in the fission yeast *S. pombe*.

445 Conversely, the *Arabidopsis* Sororin relative is an important factor for plant viability  
446 and vigor. *Atsororin* mutant plants are underrepresented in segregating populations due  
447 to compromised male, but not female, transmission of the mutant allele. The few plants  
448 that develop with a homozygous *Atsororin* mutation are dwarfed, have a short and  
449 distorted root and are sterile. Interestingly, among the somatic tissues analyzed, only  
450 roots show a strong chromosome mis-segregation phenotype, while other tissues are  
451 less affected. Somatic cells from inflorescences show hardly any mis-segregation but a  
452 widening of centromeric distances in prophase/pro-metaphase, compatible with



453 AtSORORIN's role in limiting WAPL's activity. *Atsororin* plants are sterile and the  
454 main underlying cause appears to be premature loss of sister centromere cohesion at  
455 anaphase I during male meiosis. This is different from the defect observed in *swi1*  
456 mutants, with premature loss of sister chromatid cohesion in early meiotic prophase I<sup>58</sup>.  
457 Importantly, the somatic defects of *Atsororin* mutants and the meiotic defect of *swi1*  
458 mutants could be rescued in the absence of WAPL (*wapl1 wapl2* double mutants), while  
459 the meiotic defects of *Atsororin* could not be alleviated.

460 It is interesting to note, that a very similar phenotype compared to *Atsororin* has been  
461 observed in the acetyltransferase mutant *CTF7*<sup>36</sup>, a relative of Eco1 and ESCO1/2<sup>31,68</sup>.  
462 Eco1/CTF7 acetylates the cohesin subunit SMC3 during DNA replication, thereby  
463 promoting recruitment of SORORIN and antagonizing the function of WAPL<sup>38-40</sup>. In  
464 plants, inactivation of WAPL in a *ctf7* mutant background restores somatic growth but  
465 fails to fully rescue the *ctf7* fertility defect<sup>37</sup>. These results indicate that first,  
466 AtSORORIN and AtCTF7 may act in the same pathway to promote sister chromatid  
467 cohesion by antagonizing WAPL, and second, that the dramatic dwarf phenotype  
468 observed in the single *Atsororin* and *ctf7* mutants is not a direct effect of the respective  
469 mutation, but an indirect, possibly mediated by altered cohesin dynamics.

470 Sororin has initially been perceived as the only WAPL antagonist in vertebrates<sup>40</sup>, but  
471 later the histone kinase Haspin has also been described as a WAPL antagonist with  
472 respect to cohesive cohesin<sup>69,70</sup>. It is interesting to note that loop extruding cohesin is  
473 also protected from WAPL by CTCF<sup>71,72</sup>. Haspin has been implicated in centromeric  
474 localization of the chromosome passenger complex (CPC) which plays a crucial role in  
475 chromosome bi-orientation by correcting erroneous microtubule attachment<sup>73</sup>.  
476 Localization of the CPC relies on histone H3-T3 phosphorylation, which is mediated by  
477 the histone kinase Haspin/Hrk1<sup>74-76</sup>. Hrk1/Haspin localization to centromeres depends  
478 on its interaction with Pds5<sup>70,77,78</sup>.

479 In this sense, the protein PDS5 has emerged as a central regulator for the orchestration  
480 of cohesin dynamics. Via its conserved A P D/E A P motif<sup>44,78</sup>, it can interact with  
481 diverse regulators. In human cells, PDS5 utilises this motif to interact with WAPL,  
482 HASPIN and SORORIN. Importantly, the three proteins share a common PDS5-  
483 interaction motif (PIM: K/R T/S Y S R K/L) and compete for PDS5 binding<sup>44,69,70</sup>.  
484 Furthermore, *S. pombe* Pds5 has been characterized to interact with Wpl1, Hrk1 and  
485 Eso1 (with the latter two inhibiting cohesin removal)<sup>78</sup>. Also these three proteins have a

486 common Pds5-interaction motif<sup>78</sup> and compete for the same binding domain on Pds5.  
487 Here we demonstrate that yet another protein, Sor1, can interact with Pds5, potentially  
488 also competing for the same binding platform.

489 *Arabidopsis* has five *PDS5* genes<sup>34</sup>, of which three encode PDS5 variants with a  
490 perfectly conserved interaction motif. The two *A. thaliana* WAPL proteins have well  
491 conserved PIMs at their N-termini (R T Y G R R) and are very likely direct interaction  
492 partners of PDS5 proteins, with experimental proof for the WAPL1-PDS5A pair<sup>58</sup>.

493 Common to all SORORIN proteins is the Sororin domain<sup>60</sup>. Previously it was shown to  
494 be important for interaction with cohesin complexes (SA2) and the maintenance of  
495 sister chromatid cohesion<sup>59,60</sup>. The Sororin domain is well-conserved in the *A. thaliana*  
496 and in *S. pombe* relatives, yet only one phenylalanine is present within the motif of the  
497 latter. We established in *S. pombe* that mutating this residue (F299) to alanine is as  
498 detrimental as a complete deletion of the *sor1* gene.

499 Interestingly, while we could not identify a putative PIM in the *A. thaliana* Haspin  
500 protein we noticed a well-conserved Sororin domain (Y F R D I D A F E), which is not  
501 present in Haspin proteins from other organisms. In this sense, plant Haspin may be  
502 localised to cohesin via interacting with the SCC3 subunit and may also play a role as  
503 WAPL antagonist in plants.

504 Importantly, our study provides the first organismal *in vivo* evidence that SORORIN  
505 antagonizes WAPL. We conclude (1) that orthologs of SORORIN are wide-spread in  
506 eukaryotes including yeast and plant species; (2) that plants encode more than one  
507 WAPL antagonist, and (3) that they act in clearly defined tissue and developmental  
508 contexts; and (4) that AtSORORIN may have acquired, similar to *Drosophila*'s  
509 Dalmatian, additional WAPL-independent functions in sister centromere protection at  
510 the meiosis I to meiosis II transition.

## 511 **Material and methods**

### 512 Bioinformatic analyses

513 Sororin orthologs are characterized by a very short domain at the C-terminus, which is  
514 shared between mammals and insects. This region consists of a stretch of positively  
515 charged amino acids, a polar linker (varies in size between 10 and 20 amino acids) and a  
516 conserved motif predicted to form two alpha helices and a beta strand <sup>40</sup>. We could not  
517 expand the Sororin protein family to other taxonomic clades such as fungi or plants  
518 when we considered only statistically significant hits (e-value 1e-2, data not shown). To  
519 identify candidates in other model organisms we used a hidden Markov model (HMM)  
520 of the C-terminal region (covering the *Homo sapiens* Sororin protein  
521 gi|18087845|ref|NP\_542399.1|: 216-252) and searched specifically in the proteomes of  
522 *Saccharomyces cerevisiae* and *Schizosaccharomyces pombe* (HMMER suite version  
523 2.3.2) <sup>79</sup>. We received 26 (*S. cerevisiae*) and 28 (*S. pombe*) hits with low significant e-  
524 values between 0.78 and 10. The hits were manually filtered according to the following  
525 criteria: location of the alignment at the C-terminus, conservation of the hydrophobic  
526 pattern (especially the phenylalanine residues), and no overlap with known functional  
527 domains. In budding yeast, no hit fulfilled all these criteria. In fission yeast, the best hit  
528 was to the protein SPAC9E9.05.1 (e-value 1, score -4.0). The protein is 313 residues  
529 long and the HMM alignment spanned from 241 to 310. SPAC9E9.05.1 is specific to  
530 the *Schizosaccharomyces* genus - no other orthologs could be detected with a NCBI-  
531 blastp search (version 2.2.26) <sup>80</sup> besides in *Schizosaccharomyces cryophilus*,  
532 *Schizosaccharomyces octosporus*, and *Schizosaccharomyces japonicus*. The  
533 conservation within the SPAC9E9.05 protein family is very poor (overall *S. pombe* and  
534 *S. japonicus* are only 23% identical), the C-terminus being the highest conserved region  
535 (30% identical). No known functional domains could be detected in the PFAM  
536 database. We incorporated the SPAC9E9.05.1 *Schizosaccharomyces* sequences into the  
537 HMM model and extended the search to other fungi species. In the proteome of the  
538 ascomycete *Pyrenophora tritici-repentis* (strain Pt-1C-BFP), the best hit was to a  
539 predicted protein (gi|189210197|ref|XP\_001941430.1|, score 13.5, e-value 0.089)  
540 belonging to an uncharacterized protein family that is conserved within the  
541 *Pezizomycotina* clade.

542 We confined the HMM-model to a region with highest conservation (*S. pombe*  
543 SPAC9E9.05.1: 298-311), using only fungi proteins, and searched specifically in

544 *Saccharomyces* species. In *Lipomyces starkeyi*, the best hit was significant  
545 (jgi|Lipst1\_1|72111|Locus1483v3rpkm29.51, e-value 0.0041, score 20.9) and located at  
546 the c-terminus as well. Similarly, in the *Yarrowia lipolytica* proteome we selected  
547 YALI0C19756p (e-value 0.03, score 17.7). However, no candidate could be identified  
548 in *Saccharomyces cerevisiae* or in *Candida species*.

549 To identify plant candidates, we used the same HMM model as for the *S. pombe* screen  
550 before and searched within the *Arabidopsis thaliana* proteome. The best hit was to an  
551 unknown protein (AT3G56250.1, e-value 0.04, score 14.7), which is a member of a  
552 plant specific protein family. Like for the Sororin family and the fungi candidates, the  
553 highest conservation lies in the C-terminal region. Except for some plant species, such  
554 as *Oryza sativa Japonica*, only one candidate gene was identified per genome.

555 The proteomes used in this study were retrieved from the NCBI-protein database  
556 (<http://www.ncbi.nlm.nih.gov/protein>) besides for *Saccharomyces cerevisiae*  
557 (<http://www.yeastgenome.org/>), *Schizosaccharomyces pombe*  
558 (<http://www.pombase.org/>), *Lipomyces starkeyi* ([http://genome.jgi.doe.gov/Lipst1\\_1](http://genome.jgi.doe.gov/Lipst1_1))  
559 and *Arabidopsis thaliana* (<http://www.arabidopsis.org/>).

560 Multiple alignments were performed with MAFFT (version 7, L-INS-I method)<sup>81</sup>,  
561 secondary structure prediction with Jpred (v4)<sup>82</sup>; and analyzed in Jalview<sup>83</sup>.

#### 562 *S. pombe* methods

563 The genotypes of *S. pombe* strains used in this study are listed in Table 1. Standard YES  
564 media were used to grow *S. pombe* strains strains<sup>84-86</sup>. Tagging and deletion of *S.*  
565 *pombe* genes was performed according to our protocols described in<sup>87</sup> and<sup>88</sup>,  
566 respectively. The immunofluorescence and microscopy techniques used to analyze  
567 chromosome segregation were performed as described in<sup>89</sup>. Point mutations in the *sor1*  
568 gene (to yield sor1-F299A, sor1-V302A, sor1-D303A and sor1-Y305A variants  
569 proteins) were introduced into the cloned *sor1* gene using the QuikChangeII kit (Agilent  
570 Technologies) and inserted into the genome by transformation.

571 For Western blot analyses, proteins were separated by electrophoresis through 12%  
572 polyacrylamide gels containing SDS (0.1%) and transferred to a PVDF membrane  
573 (Millipore). The membrane was blocked with 2% (w/v) milk-PBS-T (phosphate buffer  
574 saline buffer with 0.1% (v/v) Tween-20) and probed with antibodies. TAP-tagged

575 proteins were detected using rabbit antiperoxidase antibody linked to peroxidase (PAP,  
576 Dako; 1:10000 dilution). Tubulin was detected using mouse-anti- $\alpha$ -tubulin antibody  
577 (Sigma-Aldrich T5168; 1:10000 dilution) and rabbit anti-mouse IgG-HRP secondary  
578 antibody (Santa Cruz Biotechnology; 1:5000 dilution). GFP-tagged proteins were  
579 detected using mouse anti-GFP antibody (Roche 1814460, 1:1000 dilution) and anti-  
580 mouse-HRP antibody (Amersham, 1:5000). PK-tagged proteins were detected using  
581 mouse-anti-PK (V5) antibody (Serotec; 1:2000 dilution) and goat anti-mouse IgG-HRP  
582 secondary antibody (Santa Cruz Biotechnology; 1:5000 dilution) in 0.1% PBS-T. Myc-  
583 tagged proteins were detected using rabbit c-Myc antiserum (CM-100, Gramsch,  
584 Germany, 1:10000 dilution) and secondary mouse anti-rabbit-IgG antibody conjugated  
585 to HRP (sc-2357, Santa Cruz Biotechnology, 1:20000 dilution).

586 For coimmunoprecipitation, 10 ml of exponentially growing cells were collected,  
587 washed and lysed in 300  $\mu$ L of IPP150 buffer [50 mM Tris-Cl (pH=8.0), 150 mM NaCl,  
588 10% glycerol, 0.1% NP-40, 1 mM PMSF and complete EDTA-free protease inhibitors]  
589 using glass beads as described in <sup>90</sup>. The lysates were centrifuged and subjected to  
590 affinity purification via binding to anti-V5 agarose beads (Sigma-Aldrich) for 1 hour at  
591 4°C. After washing with IPP150 buffer (3x1.5 ml), the bound proteins were released by  
592 the addition of SDS-PAGE sample buffer at 95°C for 3 min. The presence of tagged  
593 proteins in the immunoprecipitates was detected by Western blot analysis as described  
594 above.

595 *In vitro* APC/C assay in *Xenopus* egg extracts was performed as previously described <sup>40</sup>.

#### 596 Plant mutant lines and growth conditions

597 The *Arabidopsis thaliana* Columbia (Col-0) ecotype was used as wild-type reference.  
598 *Atsororin* mutant plants were generated via CRISPR-Cas9 (see below). The *wapl1-1*  
599 *wapl2* double mutant (SALK\_108385, SALK\_127445) <sup>35</sup> was crossed with  
600 heterozygous *AtSORORIN* +/- mutant to obtain the *Atsororin wapl1-1 wapl2* triple  
601 mutant. Plants were grown on soil or in media plates containing Murashige and Skoog  
602 agar medium <sup>91</sup> with 2% sucrose. Long day growth conditions were applied with cycles  
603 of 16 hours light and 8 hours dark, at 21°C and 60% humidity.

604 Leaves from rosette-stage plants grown on soil or the first true leaves from seedlings  
605 grown on plates, were collected for DNA isolation and genotyping. Mutants were

606 confirmed by PCR using the primers listed below (Table 2). *Atsororin* mutants were  
607 confirmed by Sanger Sequencing of the PCR product.

#### 608 Floral dip transformation of *A. thaliana*

609 *Arabidopsis* was transformed via *Agrobacterium tumefaciens* mediated DNA transfer.  
610 In brief, an aliquot of *A. tumefaciens* electroporation-competent cells was thawed on ice  
611 and 100 ng of plasmid were added. After 15 minutes incubation on ice, the cells were  
612 transferred to electroporation cuvettes (Eppendorf, 4307-000-593). After electroporation  
613 (400  $\Omega$ , 25  $\mu$ F, 2.5 kV), 900  $\mu$ L of SOC media were added to the cuvettes and cells  
614 were left to rest for 1 hour at RT. 300  $\mu$ L of transformed cells were plated on 2xTY  
615 plates supplemented with 50  $\mu$ g/ml gentamycin, 50  $\mu$ g/ml rifampicin and 100  $\mu$ g/ml  
616 kanamycin (plasmid selection). Plates were left at 30°C overnight.

617 A single colony from transformed *Agrobacterium tumefaciens* was inoculated into 500  
618 mL of 2xTY medium supplemented with antibiotics. After 2 days rotating at 30°C, cells  
619 were centrifuged at 4500g for 30 minutes at 4°C. The pellet was then resuspended in  
620 200 mL infiltration buffer (5% sucrose in dH<sub>2</sub>O). Another centrifugation at 4500g for  
621 30 minutes at 4°C was performed and cells were now resuspended in 200 mL  
622 infiltration buffer containing 40  $\mu$ L Silwet-L77. Prior to dipping the plants into the  
623 solution, their already developed siliques and open flowers were removed. Plants were  
624 then dipped into the *Agrobacterium*/infiltration buffer solution for 30 seconds and  
625 wrapped into plastic bags afterwards to avoid fast drying of the bacterial solution. Plants  
626 were transferred to the growth chamber and two days later the bags were removed.

#### 627 *Atsororin* mutant generation

628 The *Atsororin* mutant was generated by using the CRISPR-CAS9 technology. The  
629 gRNA sequence 5'-CCGTCGGAGGAAGAATACAG-3' is specific to exon 1 of the  
630 *ATSORORIN* gene (At3g56250) and induces cleavage a few nucleotides downstream of  
631 the ATG codon. The gRNA was cloned into pGGE000-EF\_pChimera2, and together  
632 with the Cas9 promoter in pGGA000-AB\_PcUbi, the Cas9 version in pGGB000-  
633 BC\_PuCas9 and the Cas9 terminator in pGGC000-CD\_PeaTer further subcloned into  
634 the destination vector pGGZ003 utilizing the GOLDENGATE technique. The final  
635 plasmid was used to transform *Col-0* plants by using the floral dip method<sup>92</sup>.  
636 Transgenic plants grown on soil were identified and selected by their resistance to the  
637 herbicide Basta (applied by spraying 13.5 mg/l). For subsequent generations we

638 screened for the absence/presence of the BASTA resistance gene (*PAT*) using the  
639 primers 35Sp\_Fwd and Basta\_Rev. Offspring of the initial transformants with or  
640 without the transgene were analysed for the presence of a mutation in the first exon 1 of  
641 the *AtSORORIN* gene. To do so, PCR amplicons were generated using the primers  
642 Sororin\_gen0\_Fwd and Sororin\_gen0\_Rev and subsequently sequenced with the primer  
643 Sororin\_sequencing (Table 2). Plants with a mutation signature were grown for one or  
644 two more generations to identify individuals that inherited the mutation. We finally  
645 obtained a line without transgene and a stable heterozygous mutation in the  
646 *AtSORORIN* gene (Figure 1). The *Atsororin* mutant line contains a 5bps deletion within  
647 the first exon, 25 nucleotides down-stream of the ATG start codon. It results in a  
648 premature TAA stop codon after generating a short peptide of 18 amino acid residues.

#### 649 Complementation of *Atsororin* mutation

650 For complementing the *Atsororin* mutation, we first amplified the wild type  
651 *AtSORORIN* genomic version of the gene by PCR using Phusion DNA Polymerase. The  
652 primers specific for the amplification are listed in Table 2. The amplicon was then  
653 cloned into the pCB302 vector<sup>93</sup>, which is compatible with *A. tumefaciens*  
654 transformation and contains the BASTA resistance gene for future plant selection.  
655 Heterozygote *AtSORORIN* +/- plants were transformed with the pCB302 vector  
656 containing the *AtSORORIN* gene by the floral dip method to obtain the T1 generation of  
657 transformant plants. Two weeks old plants were selected for positive transformants by  
658 spraying the herbicide BASTA (150 mg/L BASTA in H<sub>2</sub>O). Heterozygote *AtSORORIN*  
659 +/- plants (based on sequencing) and BASTA-resistant were selected for three more  
660 generations. The offspring of several F3 plants were sown on soil to check their  
661 genotype. The analyzed *Atsororin* complementation lines were those that only generated  
662 offspring containing the *Atsororin* mutant allele and the complementing transgene  
663 (parent plants were homozygous for both, the *Atsororin* mutant allele and the  
664 complementing transgene).

#### 665 Seed counts

666 Mature but still green siliques originating from the fifth to the thirtieth flower per stem  
667 were harvested into fixing solution (1 part of glacial acetic acid and 3 parts of 96%  
668 EtOH) for distaining. After one day, the solution was renewed and seeds inside siliques  
669 were counted manually under a binocular microscope.

670 Alexander staining<sup>94</sup>

671 For pollen viability assays, the anthers and pollens from mature flowers were dissected  
672 under the microscope. The individual anthers were placed on a slide and a few drops  
673 (~20 µl) of Alexander staining buffer (500 µl of water, 250 µl of 87% glycerin, 100 µl  
674 of 96% Ethanol, 50 µl of 1% acid fuchsin, 10 µl of 1% malachite green, 5 µl of 1%  
675 orange G, 50 µl of glacial acetic acid) were added. The anthers were covered with a  
676 coverslip and the microscopic slide was then incubated at 50°C overnight. Stained  
677 pollen grains were observed with a microscope equipped with a differential contrast  
678 interference microscopy optics. Viable pollen grains appear round, filled with red-  
679 stained cytoplasm and coated with a thin green layer, while non-viable pollen appear  
680 only green, often shriveled and lack red cytoplasm.

681 Spreading of nuclei, fluorescence *in situ* hybridisation (FISH) and immunolocalization  
682 of meiotic proteins

683 For somatic cell preparations, the tissue of interest was fixed in Carnoy's fixative (1 part  
684 of glacial acetic acid and 3 parts of 96% EtOH). After washings twice with TRIS buffer  
685 (10mM TRIS pH 7.5, 10mM EDTA, 100mM NaCl), the plant material was disrupted  
686 with a plastic pestle in Lysis buffer (15mM TRIS pH7.5, 0,5mM spermine, 2mM  
687 EDTA, 80mM KCl, 20mM NaCl, 0,1% Triton X-100). The solution was then pipetted  
688 through a 40-micron cell strainer and centrifuged at 500g for 3 minutes. The pellet was  
689 resuspended in 50 µL of lysis buffer and pipetted to a glass slide to let air-dry. In order  
690 to visualize meiotic progression, anther spreads were prepared as described in<sup>95</sup>.

691 Fluorescence *in situ* hybridization (FISH) was performed as described in<sup>96</sup>. In brief,  
692 slides with somatic or meiotic nuclei were washed twice with 2xSSC for 5 minutes.  
693 After 10 minutes in 4% paraformaldehyde, slides were quickly washed in water and  
694 transferred through an ethanol series (70%, 90% and 96% EtOH) and then left to dry. A  
695 Locked Nucleic Acid (LNA) probe was used to detect centromere regions (5'-  
696 TTGGCTACACCATGAAAGCTT-3'; Qiagen). 20 µL of probe mix (250 nM LNA  
697 probe, 10% dextran sulfate, 50% formamide in 2 x Saline Sodium Citrate) were pipetted  
698 on the slide. A coverslip was applied, and the slides were placed on a hot plate at 75°C  
699 for 4 minutes. After an overnight incubation at 37°C, the slides were washed twice in  
700 2xSSC and 15 µL of 2 µg/ml 4',6 diamidino-2-phenylindol (DAPI) diluted in  
701 Vectashield (Vector Laboratories) were applied.

702 Spreads of nuclei for the detection of meiotic chromatin and associated proteins were



703 performed as previously described<sup>97</sup>. Primary antibodies were used as follows: 1:10000  
704 anti-ASY1 raised in guinea pig<sup>96</sup>, 1:500 anti-ZYP1 raised in rat<sup>98</sup>, 1:500 anti-SCC3  
705 raised in rabbit<sup>99</sup> and 1:250 anti-REC8 raised in rabbit<sup>100</sup>. The secondary antibodies  
706 are all commercially available and were used as follows: anti-guinea pig conjugated to  
707 Alexa Fluor 488 (1:400), anti-rabbit conjugated to Alexa Fluor 568 (1:400) and anti-rat  
708 conjugated to Alexa Fluor 647 (1:200).  
709 Images were obtained with a Zeiss Axioplan microscope (Zeiss, Oberkochen, Germany)  
710 using a Quantix<sup>®</sup> CCD camera (Photometrics, Tucson, U.S.A.). Picture acquisition was  
711 performed with MetaMorph<sup>®</sup> Microscopy Automation & Image Analysis software  
712 (Molecular Devices, Sunnyvale, U.S.A.). For meiotic prophase nuclei, Z-stacks with  
713 100 nm intervals were acquired. Deconvolution was performed using AutoQuant  
714 software (Media Cybernetics Inc, Rockville, U.S.A.) and projections were done using  
715 Helicon Focus software (HeliconSoft, Kharkov, Ukraine).

#### 716 Root tip image processing

717 Whole roots from 2-weeks old plants grown on plates were collected from different  
718 genotypes and immersed in a solution of 10 µg/mL DAPI with 0,1% Triton-X100. After  
719 30 minutes incubation at room temperature, roots were placed on a slide.  
720 Imaging was performed with a Zeiss LSM710 microscope equipped with an AiryScan  
721 Unit. To generate the movies, Z-stacks with 250 nm intervals were acquired.  
722 Deconvolution was performed with the Huygens Software.

#### 723 Statistical analyses

724 All statistical analyses were performed using the GraphPad Prism 7 software. First,  
725 D'Agostino-Pearson omnibus normality test was performed to analyze if the data  
726 followed a Gaussian distribution. If yes, the two variables were compared using  
727 unpaired t-test. When no Gaussian distribution was detected, unpaired Mann-Whitney  
728 tests were applied. Contingency tables were generated to compare expected (or wild  
729 type) data with mutant values. Fischer's exact test was used when two variables were  
730 compared. For three or more variables, Chi-square tests were performed.

731 **References**

- 732 1. Ishiguro, K. ichiro. The cohesin complex in mammalian meiosis. *Genes to Cells* vol. 24 6–30  
733 (2019).
- 734 2. Oldenkamp, R. & Rowland, B. D. A walk through the SMC cycle: From catching DNAs to shaping  
735 the genome. *Molecular Cell* vol. 82 1616–1630 (2022).
- 736 3. Haering, C. H., Farcas, A. M., Arumugam, P., Metson, J. & Nasmyth, K. The cohesin ring  
737 concatenates sister DNA molecules. *Nature* **454**, 297–301 (2008).
- 738 4. Peters, J. M., Tedeschi, A. & Schmitz, J. The cohesin complex and its roles in chromosome  
739 biology. *Genes Dev.* **22**, 3089–3114 (2008).
- 740 5. Davidson, I. F. & Peters, J. M. Genome folding through loop extrusion by SMC complexes. *Nature*  
741 *Reviews Molecular Cell Biology* vol. 22 445–464 (2021).
- 742 6. Tomonaga, T. *et al.* Characterization of fission yeast cohesin: Essential anaphase proteolysis of  
743 Rad21 phosphorylated in the S phase. *Genes Dev.* **14**, 2757–2770 (2000).
- 744 7. Schubert, V. SMC proteins and their multiple functions in higher plants. *Cytogenetic and*  
745 *Genome Research* vol. 124 202–214 (2009).
- 746 8. Schleiffer, A. *et al.* Kleisins: A superfamily of bacterial and eukaryotic SMC protein partners. *Mol.*  
747 *Cell* **11**, 571–575 (2003).
- 748 9. Gligoris, T. G. *et al.* Closing the cohesin ring: Structure and function of its Smc3-kleisin interface.  
749 *Science (80-. ).* **346**, 963–967 (2014).
- 750 10. Sonoda, E. *et al.* Scc1/Rad21/Mcd1 Is Required for Sister Chromatid Cohesion and Kinetochores  
751 Function in Vertebrate Cells. *Dev. Cell* **1**, 759–770 (2001).
- 752 11. Hu, B. *et al.* ATP hydrolysis is required for relocating cohesin from sites occupied by its Scc2/4  
753 loading complex. *Curr. Biol.* **21**, 12–24 (2011).
- 754 12. Orgil, O. *et al.* A Conserved Domain in the Scc3 Subunit of Cohesin Mediates the Interaction with  
755 Both Mcd1 and the Cohesin Loader Complex. **11**, e1005036 (2015).
- 756 13. Hauf, S. *et al.* Dissociation of cohesin from chromosome arms and loss of arm cohesion during  
757 early mitosis depends on phosphorylation of SA2. *PLoS Biol.* **3**, (2005).
- 758 14. Roig, M. B. *et al.* Structure and function of cohesin’s Scc3/SA regulatory subunit. *FEBS Lett.* **588**,  
759 3692–3702 (2014).
- 760 15. Li, Y. *et al.* Structural basis for scc3-dependent cohesin recruitment to chromatin. *Elife* **7**, (2018).
- 761 16. Murayama, Y. & Uhlmann, F. Biochemical reconstitution of topological DNA binding by the  
762 cohesin ring. *Nature* **505**, 367–371 (2014).
- 763 17. Wells, J. N., Gligoris, T. G., Nasmyth, K. A. & Marsh, J. A. Evolution of condensin and cohesin  
764 complexes driven by replacement of Kite by Hawk proteins. *Current Biology* vol. 27 R17–R18  
765 (2017).
- 766 18. Petela, N. J. *et al.* Scc2 Is a Potent Activator of Cohesin’s ATPase that Promotes Loading by  
767 Binding Scc1 without Pds5. *Mol. Cell* **70**, 1134–1148.e7 (2018).
- 768 19. Kikuchi, S., Borek, D. M., Otwinowski, Z., Tomchick, D. R. & Yu, H. Crystal structure of the cohesin  
769 loader Scc2 and insight into cohesinopathy. *Proc. Natl. Acad. Sci. U. S. A.* **113**, 12444–12449  
770 (2016).
- 771 20. Davidson, I. F. *et al.* DNA loop extrusion by human cohesin. *Science (80-. ).* **366**, 1338–1345  
772 (2019).

- 773 21. Kim, Y., Shi, Z., Zhang, H., Finkelstein, I. J. & Yu, H. Human cohesin compacts DNA by loop  
774 extrusion. *Science (80-. )*. **366**, 1345–1349 (2019).
- 775 22. Ciosk, R. *et al.* Cohesin's binding to chromosomes depends on a separate complex consisting of  
776 Scc2 and Scc4 proteins. *Mol. Cell* **5**, 243–254 (2000).
- 777 23. Kueng, S. *et al.* Wapl Controls the Dynamic Association of Cohesin with Chromatin. *Cell* **127**,  
778 955–967 (2006).
- 779 24. Beckouët, F. *et al.* Releasing Activity Disengages Cohesin's Smc3/Scc1 Interface in a Process  
780 Blocked by Acetylation. *Mol. Cell* **61**, 563–574 (2016).
- 781 25. Chan, K. L. *et al.* Cohesin's DNA exit gate is distinct from its entrance gate and is regulated by  
782 acetylation. *Cell* **150**, 961–974 (2012).
- 783 26. Huis In't Veld, P. J. *et al.* Characterization of a DNA exit gate in the human cohesin ring. *Science*  
784 *(80-. )*. **346**, 968–972 (2014).
- 785 27. Gerlich, D., Koch, B., Dupeux, F., Peters, J. M. & Ellenberg, J. Live-Cell Imaging Reveals a Stable  
786 Cohesin-Chromatin Interaction after but Not before DNA Replication. *Curr. Biol.* **16**, 1571–1578  
787 (2006).
- 788 28. Bernard, P. *et al.* Cell-cycle regulation of cohesin stability along fission yeast chromosomes.  
789 *EMBO J.* **27**, 111–121 (2008).
- 790 29. Ben-Shahar, T. R. *et al.* Eco1-dependent cohesin acetylation during establishment of sister  
791 chromatid cohesion. *Science (80-. )*. **321**, 563–566 (2008).
- 792 30. Ivanov, D. *et al.* Eco1 is a novel acetyltransferase that can acetylate proteins involved in  
793 cohesion. *Curr. Biol.* **12**, 323–328 (2002).
- 794 31. Tóth, A. *et al.* Yeast cohesin complex requires a conserved protein, Eco1p(Ctf7), to establish  
795 cohesion between sister chromatids during DNA replication. *Genes Dev.* **13**, 320–333 (1999).
- 796 32. Ünal, E. *et al.* A molecular determinant for the establishment of sister chromatid cohesion.  
797 *Science (80-. )*. **321**, 566–569 (2008).
- 798 33. Zhang, J. *et al.* Acetylation of Smc3 by Eco1 Is Required for S Phase Sister Chromatid Cohesion in  
799 Both Human and Yeast. *Mol. Cell* **31**, 143–151 (2008).
- 800 34. Pradillo, M. *et al.* Involvement of the cohesin cofactor PDS5 (SPO76) during meiosis and DNA  
801 repair in *Arabidopsis thaliana*. *Front. Plant Sci.* **6**, 1034 (2015).
- 802 35. De, K., Sterle, L., Krueger, L., Yang, X. & Makaroff, C. A. *Arabidopsis thaliana* WAPL Is Essential for  
803 the Prophase Removal of Cohesin during Meiosis. *PLoS Genet.* **10**, e1004497 (2014).
- 804 36. Bolaños-Villegas, P. *et al.* *Arabidopsis* CHROMOSOME TRANSMISSION FIDELITY 7 (AtCTF7/ECO1)  
805 is required for DNA repair, mitosis and meiosis. *Plant J.* **75**, 927–940 (2013).
- 806 37. De, K. *et al.* The opposing actions of *Arabidopsis* CHROMOSOME TRANSMISSION FIDELITY7 and  
807 WINGS APART-LIKE1 and 2 differ in mitotic and meiotic cells. *Plant Cell* **28**, 521–536 (2015).
- 808 38. Lafont, A. L., Song, J. & Rankin, S. Sororin cooperates with the acetyltransferase Eco2 to ensure  
809 DNA replication-dependent sister chromatid cohesion. *Proc. Natl. Acad. Sci. U. S. A.* **107**, 20364–  
810 20369 (2010).
- 811 39. Song, J. *et al.* Cohesin acetylation promotes sister chromatid cohesion only in association with  
812 the replication machinery. *J. Biol. Chem.* **287**, 34325–34336 (2012).
- 813 40. Nishiyama, T. *et al.* Sororin mediates sister chromatid cohesion by antagonizing Wapl. *Cell* **143**,  
814 737–749 (2010).
- 815 41. Yamada, T., Tahara, E., Kanke, M., Kuwata, K. & Nishiyama, T. *Drosophila* Dalmatian combines  
816 sororin and shugoshin roles in establishment and protection of cohesion. *EMBO J.* **36**, 1513–

- 817 1527 (2017).
- 818 42. Rankin, S., Ayad, N. G. & Kirschner, M. W. Sororin, a substrate of the anaphase- promoting  
819 complex, is required for sister chromatid cohesion in vertebrates. *Mol. Cell* **18**, 185–200 (2005).
- 820 43. Schmitz, J., Watrin, E., Lénárt, P., Mechtler, K. & Peters, J. M. Sororin Is Required for Stable  
821 Binding of Cohesin to Chromatin and for Sister Chromatid Cohesion in Interphase. *Curr. Biol.* **17**,  
822 630–636 (2007).
- 823 44. Ouyang, Z., Zheng, G., Tomchick, D. R., Luo, X. & Yu, H. Structural Basis and IP6 Requirement for  
824 Pds5-Dependent Cohesin Dynamics. *Mol. Cell* **62**, 248–259 (2016).
- 825 45. Ladurner, R. *et al.* Sororin actively maintains sister chromatid cohesion. *EMBO J.* **35**, 635–653  
826 (2016).
- 827 46. Waizenegger, I. C., Hauf, S., Meinke, A. & Peters, J. M. Two distinct pathways remove  
828 mammalian cohesin from chromosome arms in prophase and from centromeres in anaphase.  
829 *Cell* **103**, 399–410 (2000).
- 830 47. Buheitel, J. & Stemann, O. Prophase pathway-dependent removal of cohesin from human  
831 chromosomes requires opening of the Smc3-Scc1 gate. *EMBO Journal* vol. 32 666–676 (2013).
- 832 48. Gandhi, R., Gillespie, P. J. & Hirano, T. Human Wapl Is a Cohesin-Binding Protein that Promotes  
833 Sister-Chromatid Resolution in Mitotic Prophase. *Curr. Biol.* **16**, 2406–2417 (2006).
- 834 49. Zhang, N., Panigrahi, A. K., Mao, Q. & Pati, D. Interaction of sororin protein with polo-like kinase  
835 1 mediates resolution of chromosomal arm cohesion. *J. Biol. Chem.* **286**, 41826–41837 (2011).
- 836 50. Dreier, M. R., Bekier, M. E. & Taylor, W. R. Regulation of sororin by cdk1-mediated  
837 phosphorylation. *J. Cell Sci.* **124**, 2976–2987 (2011).
- 838 51. Nishiyama, T., Sykora, M. M., Huis, P. J., Mechtler, K. & Peters, J. M. Aurora B and Cdk1 mediate  
839 Wapl activation and release of acetylated cohesin from chromosomes by phosphorylating  
840 Sororin. *Proc. Natl. Acad. Sci. U. S. A.* **110**, 13404–13409 (2013).
- 841 52. Liu, H., Rankin, S. & Yu, H. Phosphorylation-enabled binding of SGO1-PP2A to cohesin protects  
842 sororin and centromeric cohesion during mitosis. *Nat. Cell Biol.* **15**, 40–49 (2013).
- 843 53. Kitajima, T. S. *et al.* Shugoshin collaborates with protein phosphatase 2A to protect cohesin.  
844 *Nature* **441**, 46–52 (2006).
- 845 54. Hornig, N. C. D., Knowles, P. P., McDonald, N. Q. & Uhlmann, F. The dual mechanism of separase  
846 regulation by securin. *Curr. Biol.* **12**, 973–982 (2002).
- 847 55. Hagting, A. *et al.* Human securin proteolysis is controlled by the spindle checkpoint and reveals  
848 when the APC/C switches from activation by Cdc20 to Cdh1. *J. Cell Biol.* **157**, 1125–1137 (2002).
- 849 56. Wirth, K. G. *et al.* Separase: A universal trigger for sister chromatid disjunction but not  
850 chromosome cycle progression. *J. Cell Biol.* **172**, 847–860 (2006).
- 851 57. Sutani, T., Kawaguchi, T., Kanno, R., Itoh, T. & Shirahige, K. Budding Yeast Wpl1(Rad61)-Pds5  
852 Complex Counteracts Sister Chromatid Cohesion-Establishing Reaction. *Curr. Biol.* **19**, 492–497  
853 (2009).
- 854 58. Yang, C. *et al.* SWITCH 1/DYAD is a WINGS APART-LIKE antagonist that maintains sister  
855 chromatid cohesion in meiosis. *Nat. Commun.* **10**, (2019).
- 856 59. Zhang, N. & Pati, D. C-terminus of sororin interacts with sa2 and regulates sister chromatid  
857 cohesion. *Cell Cycle* **14**, 820–826 (2015).
- 858 60. Wu, F. M., Nguyen, J. V. & Rankin, S. A conserved motif at the C terminus of sororin is required  
859 for sister chromatid cohesion. *J. Biol. Chem.* **286**, 3579–3586 (2011).
- 860 61. McDowall, M. D. *et al.* PomBase 2015: Updates to the fission yeast database. *Nucleic Acids Res.*

- 861           **43**, D656–D661 (2015).
- 862   62.   Feytout, A., Vaur, S., Genier, S., Vazquez, S. & Javerzat, J.-P. Psm3 Acetylation on Conserved  
863   Lysine Residues Is Dispensable for Viability in Fission Yeast but Contributes to Eso1-Mediated  
864   Sister Chromatid Cohesion by Antagonizing Wpl1. *Mol. Cell. Biol.* **31**, 1771–1786 (2011).
- 865   63.   Furuya, K., Takahashi, K. & Yanagida, M. Faithful anaphase is ensured by Mis4, a sister chromatid  
866   cohesion molecule required in S phase and not destroyed in G1 phase. *Genes Dev.* **12**, 3408–  
867   3418 (1998).
- 868   64.   Chen, Z., McCroskey, S., Guo, W., Li, H. & Gerton, J. L. A genetic screen to discover pathways  
869   affecting cohesin function in *Schizosaccharomyces pombe* identifies chromatin effectors. *G3*  
870   *Genes, Genomes, Genet.* **2**, 1161–1168 (2012).
- 871   65.   Matsuyama, A. *et al.* ORFeome cloning and global analysis of protein localization in the fission  
872   yeast *Schizosaccharomyces pombe*. *Nat. Biotechnol.* **24**, 841–847 (2006).
- 873   66.   Yatskevich, S., Rhodes, J. & Nasmyth, K. Organization of Chromosomal DNA by SMC Complexes.  
874   *Annual Review of Genetics* vol. 53 445–482 (2019).
- 875   67.   Mercier, R. *et al.* SWITCH1 (SWI1): A novel protein required for the establishment of sister  
876   chromatid cohesion and for bivalent formation at meiosis. *Genes Dev.* **15**, 1859–1871 (2001).
- 877   68.   Alomer, R. M. *et al.* Esco1 and Esco2 regulate distinct cohesin functions during cell cycle  
878   progression. *Proc. Natl. Acad. Sci. U. S. A.* **114**, 9906–9911 (2017).
- 879   69.   Zhou, L. *et al.* The N-Terminal Non-Kinase-Domain-Mediated Binding of Haspin to Pds5B  
880   Protects Centromeric Cohesion in Mitosis. *Curr. Biol.* **27**, 992–1004 (2017).
- 881   70.   Liang, C. *et al.* A kinase-dependent role for Haspin in antagonizing Wapl and protecting mitotic  
882   centromere cohesion. *EMBO Rep.* **19**, 43–56 (2018).
- 883   71.   Wutz, G. *et al.* ESCO1 and CTCF enable formation of long chromatin loops by protecting  
884   cohesinstag1 from WAPL. *Elife* **9**, (2020).
- 885   72.   Li, Y. *et al.* The structural basis for cohesin–CTCF-anchored loops. *Nature* **578**, 472–476 (2020).
- 886   73.   Haase, J., Bonner, M. K., Halas, H. & Kelly, A. E. Distinct Roles of the Chromosomal Passenger  
887   Complex in the Detection of and Response to Errors in Kinetochore-Microtubule Attachment.  
888   *Dev. Cell* **42**, 640-654.e5 (2017).
- 889   74.   Dai, J., Sultan, S., Taylor, S. S. & Higgins, J. M. G. The kinase haspin is required for mitotic histone  
890   H3 Thr 3 phosphorylation and normal metaphase chromosome alignment. *Genes Dev.* **19**, 472–  
891   488 (2005).
- 892   75.   Kurihara, D., Matsunaga, S., Omura, T., Higashiyama, T. & Fukui, K. Identification and  
893   characterization of plant Haspin kinase as a histone H3 threonine kinase. *BMC Plant Biol.* **11**,  
894   (2011).
- 895   76.   Wang, F. *et al.* Histone H3 Thr-3 phosphorylation by haspin positions Aurora B at centromeres in  
896   mitosis. *Science (80-. )*. **330**, 231–235 (2010).
- 897   77.   Yamagishi, Y., Honda, T., Tanno, Y. & Watanabe, Y. Two histone marks establish the inner  
898   centromere and chromosome bi-orientation. *Science (80-. )*. **330**, 239–243 (2010).
- 899   78.   Goto, Y. *et al.* Pds5 Regulates Sister-Chromatid Cohesion and Chromosome Bi-orientation  
900   through a Conserved Protein Interaction Module. *Curr. Biol.* **27**, 1005–1012 (2017).
- 901   79.   Eddy, S. R. Profile hidden Markov models. *Bioinformatics* vol. 14 755–763 (1998).
- 902   80.   Altschul, S. F. *et al.* Gapped BLAST and PSI-BLAST: A new generation of protein database search  
903   programs. *Nucleic Acids Research* vol. 25 3389–3402 (1997).
- 904   81.   Kato, K. & Toh, H. Recent developments in the MAFFT multiple sequence alignment program.

- 905 *Brief. Bioinform.* **9**, 286–298 (2008).
- 906 82. Drozdetskiy, A., Cole, C., Procter, J. & Barton, G. J. JPred4: A protein secondary structure  
907 prediction server. *Nucleic Acids Res.* **43**, W389–W394 (2015).
- 908 83. Waterhouse, A. M., Procter, J. B., Martin, D. M. A., Clamp, M. & Barton, G. J. Jalview Version 2-A  
909 multiple sequence alignment editor and analysis workbench. *Bioinformatics* **25**, 1189–1191  
910 (2009).
- 911 84. Cipak, L. *et al.* Generation of a set of conditional analog-sensitive alleles of essential protein  
912 kinases in the fission yeast *Schizosaccharomyces pombe*. *Cell Cycle* **10**, 3527–3532 (2011).
- 913 85. Dudas, A., Polakova, S. & Gregan, J. Chromosome segregation: Monopolin attracts condensin.  
914 *Current Biology* vol. 21 (2011).
- 915 86. Sabatinos, S. A. & Forsburg, S. L. Molecular genetics of *Schizosaccharomyces pombe*. *Methods*  
916 *Enzymol.* **470**, 759–795 (2010).
- 917 87. Cipak, L. *et al.* An improved strategy for tandem affinity purification-tagging of  
918 *Schizosaccharomyces pombe* genes. *Proteomics* **9**, 4825–4828 (2009).
- 919 88. Kovacicova, I. *et al.* A knockout screen for protein kinases required for the proper meiotic  
920 segregation of chromosomes in the fission yeast *Schizosaccharomyces pombe*. *Cell Cycle* **12**,  
921 618–624 (2013).
- 922 89. Polakova, S. *et al.* Dbl2 Regulates Rad51 and DNA Joint Molecule Metabolism to Ensure Proper  
923 Meiotic Chromosome Segregation. *PLoS Genet.* **12**, (2016).
- 924 90. Phadnis, N. *et al.* Casein Kinase 1 and Phosphorylation of Cohesin Subunit Rec11 (SA3) Promote  
925 Meiotic Recombination through Linear Element Formation. *PLoS Genet.* **11**, (2015).
- 926 91. Murashige, T. & Skoog, F. A Revised Medium for Rapid Growth and Bio Assays with Tobacco  
927 Tissue Cultures. *Physiol. Plant.* **15**, 473–497 (1962).
- 928 92. Clough, S. J. & Bent, A. F. Floral dip: A simplified method for *Agrobacterium*-mediated  
929 transformation of *Arabidopsis thaliana*. *Plant J.* **16**, 735–743 (1998).
- 930 93. Xiang, C., Han, P., Lutziger, I., Wang, K. & Oliver, D. J. A mini binary vector series for plant  
931 transformation. *Plant Mol. Biol.* **40**, 711–717 (1999).
- 932 94. Alexander, M. P. Differential staining of aborted and nonaborted pollen. *Biotech. Histochem.* **44**,  
933 117–122 (1969).
- 934 95. Vignard, J. *et al.* The Interplay of RecA-related Proteins and the MND1–HOP2 Complex during  
935 Meiosis in *Arabidopsis thaliana*. *PLoS Genet.* **3**, e176 (2007).
- 936 96. Sims, J., Copenhaver, G. P. & Schlögelhofer, P. Meiotic DNA repair in the nucleolus employs a  
937 nonhomologous end-joining mechanism. *Plant Cell* **31**, 2259–2275 (2019).
- 938 97. Kurzbauer, M. T., Uanschou, C., Chen, D. & Schlögelhofer, P. The recombinases DMC1 and  
939 RAD51 are functionally and spatially separated during meiosis in *Arabidopsis*. *Plant Cell* **24**,  
940 2058–2070 (2012).
- 941 98. Higgins, J. D., Sanchez-Moran, E., Armstrong, S. J., Jones, G. H. & Franklin, F. C. H. The  
942 *Arabidopsis* synaptonemal complex protein ZYP1 is required for chromosome synapsis and  
943 normal fidelity of crossing over. *Genes Dev.* **19**, 2488–2500 (2005).
- 944 99. Chelysheva, L. *et al.* AtREC8 and AtSCC3 are essential to the monopolar orientation of the  
945 kinetochores during meiosis. *J. Cell Sci.* **118**, 4621–4632 (2005).
- 946 100. Cromer, L. *et al.* Centromeric cohesion is protected twice at meiosis, by SHUGOSHINs at  
947 anaphase I and by PATRONUS at interkinesis. *Curr. Biol.* **23**, 2090–2099 (2013).
- 948 101. Ren, J. *et al.* DOG 1.0: Illustrator of protein domain structures. *Cell Research* vol. 19 271–273

949 (2009).

950

951 **Competing Interest**

952 The authors declare to have no competing interests.

953

954 **Acknowledgements**

955 J.G. was supported by the Austrian Science Fund (FWF) (grant P30516), the Slovak  
956 Grant Agency VEGA (1/0450/18 and 2/0026/18) and the Slovak Research and  
957 Development Agency (APVV-17-0130, APVV-18-0219, and APVV-16-0120).  
958 Research in the laboratory of P.S. was supported by the Austrian Science Fund (FWF)  
959 (I 1468-B16; Special Research Focus program “Chromosome Dynamics” F3408-B19;  
960 FWF Doctoral Program “Chromosome Dynamics” W1238-B20) and the Austria's  
961 Agency for Education and Internationalization (Ernst Mach Grant to TTN). Research in  
962 the laboratory of J.-M.P is supported by Boehringer Ingelheim, the Austrian Research  
963 Promotion Agency (Headquarter grant FFG-852936), the European Research Council  
964 under the European Union’s Horizon 2020 Research and Innovation Programme  
965 (1020558), the Human Frontier Science Program (RGP0057/2018), and the Vienna  
966 Science and Technology Fund (LS19-029). J.- M.P. is also an adjunct professor at the  
967 Medical University of Vienna. We thank Vera Schoft and the Vienna Biocenter Core  
968 Facility (PlantS) for assistance in generating the *Atsororin* mutant line. We thank M.  
969 Yanagida, J.P. Javerzat and J. Gerton for sending yeast strains and B. Huraiova, L.  
970 Cipak and S. Polakova for help with yeast experiments.

971

972 **Author Contributions**

973 A.S. and J.-M.P. performed the bioinformatic analyses and identified putative *Sororin*  
974 homologs in eukaryotes. M.G., I.K., T.N. and J.G. conceived and performed the  
975 experiments with *S. pombe*. I.P.M. and P.S. conceived and performed the experiments  
976 with *A. thaliana*. T.T.N. generated the *A. thaliana sororin* mutant. I.P.M., J.G., J.-M.P.  
977 and P.S. analyzed the data and wrote the manuscript.

978 **Figure legends**

979 **Figure 1.** *S. pombe* Sor1 and *A. thaliana* AtSORORIN share sequence similarities with  
980 metazoan Sororin proteins. **a** Domain architecture of Sororin and putative Sororin  
981 orthologs. The Sororin domain is shown in blue, the cluster of positively charged  
982 residues (lysine, arginine) in red, the KEN box in magenta and the FGF motif in yellow.  
983 The domain graphs were created with the help of the domain illustrator (DOG 2.0<sup>101</sup>). **b**  
984 Alignment of the C-terminal Sororin domain. UniProt accessions are provided next to  
985 the species names. Residues mutated in this study are indicated by asterisks. Secondary  
986 structure prediction of *H. sapiens* and *S. pombe* are shown on the top and bottom,  
987 respectively, where alpha helices are in red, and beta strands in green.

988 **Figure 2.** *S. pombe* Sor1 is involved in sister chromatid cohesion and its conserved  
989 residues are important for Sor1 function and association with cohesin. **a** *sor1Δ* cells  
990 show a weak cohesion defect which is partially suppressed by *wpl1Δ*. Wild type and  
991 *sor1Δ* haploid cells expressing *cen2*-GFP were fixed and stained with antibodies against  
992 tubulin and GFP and sister chromatid cohesion was analyzed in metaphase cells. Nuclei  
993 were visualized by Hoechst staining. Means +/- standard deviations are shown.  
994 Unpaired t-test was performed for statistical analysis (\*\*p<0.01; ns – not significant). **b**  
995 Negative synthetic growth interaction in *esolts sor1Δ* and *mis4ts sor1Δ* double mutants  
996 are associated with chromosome segregation defects. Wild type, *sor1Δ*, *esol-G799D*  
997 (*esol-ts*), *esol-G799D sor1Δ*, *mis4-242 (mis4-ts)* and *mis4-242 sor1Δ* haploid cells  
998 expressing *cen2*-GFP were fixed and stained with antibodies against tubulin and GFP.  
999 Nuclei were visualized by Hoechst staining. Samples were examined under the  
1000 fluorescence microscope, and segregation of chromosome 2 marked by *cen2*-GFP was  
1001 scored in late anaphase cells. Lagging chromosomes were identified as Hoechst-staining  
1002 bodies between the poles of the spindle in late anaphase. Means +/- standard deviations  
1003 are shown. Unpaired t-test was performed for statistical analysis (\*p<0.05; \*\*p<0.01). **c**  
1004 Pds5-Myc co-immunoprecipitates with Sor1-Pk. Protein extracts were prepared from  
1005 cycling wild type cells and cells expressing Sor1-Pk, Pds5-myc or both Sor1-Pk and  
1006 Pds5-Myc, as indicated. Proteins bound to anti-V5 agarose beads, which bind the Pk tag  
1007 on Sor1, were analyzed for Pds5-Myc by Western blotting using anti-Myc antibody. **d**  
1008 Psm3-GFP co-immunoprecipitates with Sor1-Pk and this interaction is weakened by  
1009 mutating conserved Sor1 residue D303. Protein extracts were prepared from cycling  
1010 wild type cells and cells expressing Sor1-Pk, Psm3-GFP or both Sor1-Pk and Psm3-



1011 GFP, as indicated. Proteins bound to anti-V5 agarose beads, which bind the Pk tag on  
1012 Sor1, were analyzed for Psm3-GFP by Western blotting using anti-GFP antibody.  
1013 Mutant protein Sor1-D303A-Pk co-immunoprecipitated with the Psm3-GFP protein less  
1014 efficiently, as compared to wild type Sor1-Pk. e The four conserved residues in the  
1015 Sororin domain are important for the Sor1 function. Strains with the indicated mutations  
1016 were grown on YES medium for one day. Serial dilutions were spotted onto YES plates  
1017 and incubated for 3 days at 25°C or 30°C. While expression of a wild type Sor1 rescued  
1018 the growth defect of the *esol-G799D sor1Δ* double mutant (*esol-ts sor1-wt*), mutant  
1019 Sor1 proteins carrying F299A, V302A, D303A or Y305A substitutions did not rescue  
1020 the growth defect of *esol-G799D sor1Δ* double mutants (*esol-ts sor1-F299A*, *esol-ts*  
1021 *sor1-V302A*, *esol-ts sor1-D303A*, *esol-ts sor1-Y305A*).

1022 **Figure 3.** Loss of WAPL rescues somatic defects of *Atsororin* mutants. **a** Schematic  
1023 representation of *AtSORORIN* (AT3G56250) gene, with 5' and 3' UTRs (grey boxes),  
1024 introns (black lines) and exons (black boxes), open reading frame (ATG/TAA, black),  
1025 Cas9 target site (black triangle) and premature stop codon in mutants plans (TAA, red)  
1026 indicated. **b** The severe growth restriction of homozygous *Atsororin* mutants plants  
1027 (seedlings, scale bar = 5mm; mature plants, scale bar = 5 cm) is alleviated by loss of  
1028 WAPL (*Atsororin wapl1-1 wapl2* triple mutants). Wild-type plants, *Atsororin*, *wapl1-1*  
1029 *wapl2* double mutants and *Atsororin wapl1-1 wapl2* triple mutants were grown side-by-  
1030 side for comparison. **c** Images of root tips and entire seedlings (small pictures) of plants  
1031 grown on media plates for two weeks. Root growth restriction (red bars) and loss of  
1032 characteristic layering of the root meristem in *Atsororin* mutant plants are evident.  
1033 These deficiencies are rescued by loss of WAPL (*wapl1-1 wapl2* double mutants). All  
1034 plants were grown side-by-side for comparison. Scale bar = 1 mm. **d** Quantification of  
1035 root growth of plants grown on media plates for two weeks. Unpaired Mann-Whitney  
1036 test has been applied (\* $p < 0.05$ ; \*\* $p < 0.01$ ; \*\*\*\* $p < 0.0001$ ; ns – difference not  
1037 significant). **e** Loss of fertility in *Atsororin* mutant plants is only partially rescued by  
1038 WAPL inactivation. All plants were grown side-by-side and genotypes are indicated.  
1039 Images show representative, opened siliques and developing seeds. *Atsororin wapl1-1*  
1040 *wapl2* triple mutant plants have siliques with some seeds, which are mostly bigger than  
1041 those formed in wild type-plants. Unpaired Mann-Whitney test has been applied  
1042 (\*\*\*\* $p < 0.0001$ ). Scale bar = 1 mm. **f** Genotypes of offspring of self-pollinated  
1043 *AtSORORIN* +/- plants. The homozygous *Atsororin* -/- genotype is strongly

1044 underrepresented (chi-square analysis, p value indicated). **g** Genotyping the offspring of  
1045 reciprocal crosses between *AtSORORIN* +/- and wild type plants indicates that only  
1046 male, but not female, gametogenesis, is affected by the *Atsororin* mutation (Fisher's  
1047 exact test, p values indicated). **h** Flower architecture is not affected by the lack of  
1048 *AtSORORIN* whereas anther growth and pollen viability are severely disturbed.  
1049 *Atsororin* single mutants and *Atsororin wapl1-1 wapl2* triple mutants develop smaller  
1050 anthers with few viable pollen grains. All plants were grown side-by-side and genotypes  
1051 are indicated. Scale bar flowers = 1 mm, scale bar anthers = 200  $\mu$ m.

1052 **Figure 4.** Somatic defects in *Atsororin* mutants are tissue-specific and WAPL-  
1053 dependent. DNA was stained with DAPI (magenta) and fluorescence *in situ*  
1054 hybridization (FISH) was performed to detect centromeric regions (green). **a** Spreads of  
1055 root cell nuclei. Interphase, metaphase and anaphase stages were analyzed for wild-type  
1056 plants and *Atsororin*, *wapl1-1 wapl2* and *Atsororin wapl1-1 wapl2* mutants. Scale bar =  
1057 10  $\mu$ m. **b** Quantification of centromeric-FISH signals in interphase root nuclei.  
1058 *Atsororin* mutants (n = 34) show a significantly higher number of signals than wild type  
1059 (n = 93), *wapl1-1 wapl2* (n = 73) and *Atsororin wapl1-1 wapl2* (n = 59) (chi-square  
1060 analysis; \*p<0.05; \*\*p<0.01; \*\*\*\*p<0.0001; ns – difference not significant). **c** Spreads  
1061 of somatic cell nuclei from inflorescences. Interphase, prophase, prometaphase,  
1062 metaphase and anaphase stages were analyzed for wild-type plants and *Atsororin*,  
1063 *wapl1-1 wapl2* and *Atsororin wapl1-1 wapl2* mutants. Magnifications of signals at the  
1064 sister centromeres are provided for prophase and prometaphase stages. Scale bar = 10  
1065  $\mu$ m. **d** Quantification of centromeric-FISH signals observed in nuclei of cells from  
1066 inflorescences at interphase. Quantification was performed on wild-type plants (n =  
1067 224) and *Atsororin* (n = 266), *wapl1-1 wapl2* (n = 238) and *Atsororin wapl1-1 wapl2*  
1068 mutants (n = 236) (chi-square analysis; \*\*\*\*p<0.0001; ns – difference not significant).  
1069 **e** Measurements of the physical distance between FISH signals of sister chromatid  
1070 centromeres during prophase. *Atsororin* mutants (n = 39) show a significant increase in  
1071 distance between sister centromeres when compared to wild type (n = 45), *wapl1-1*  
1072 *wapl2* (n = 37) and *Atsororin wapl1-1 wapl2* (n = 50). Unpaired t-test was performed  
1073 (\*p<0.05; \*\*\*p<0.001; \*\*\*\*p<0.0001). **f** Measurements of the physical distance  
1074 between FISH signals at sister chromatid centromeres during prometaphase. *Atsororin*  
1075 mutants (n = 55) show a significant increase in distance between sister centromeres  
1076 when compared to wild type (n = 42), *wapl1-1 wapl2* (n = 46) and *Atsororin wapl1-1*

1077 *wapl2* (n = 49). Unpaired t-test was performed (\*\*\*\*p<0.0001; ns – difference not  
1078 significant).

1079 **Figure 5.** Plants lacking AtSORORIN exhibit defects during male meiosis. Spreads of  
1080 meiotic nuclei from wild-type plants and *Atsororin*, *wapl1-1 wapl2* and *Atsororin*  
1081 *wapl1-1 wapl2* mutants. Meiotic progression until metaphase I, including homologous  
1082 chromosome pairing and bivalent formation, appears normal in all genotypes. The  
1083 number of DAPI-stained bodies is increased in mutants lacking AtSORORIN after  
1084 metaphase I, yielding 10 chromatids in prophase II. Progression through meiosis II is  
1085 therefore defective in *Atsororin* single mutants with the subsequent formation of  
1086 unbalanced tetrads. Inactivation of WAPL does not rescue chromosome non-disjunction  
1087 observed in anaphase II in the *Atsororin* single mutants. Scale bar = 10  $\mu$ m.

1088 **Figure 6.** Premature separation of centromeres during meiosis in *Atsororin* mutant  
1089 plants. Fluorescence *in situ* hybridization experiment on male meiocytes with a probe  
1090 directed against the centromeric regions (green) in wild-type plants and *Atsororin*,  
1091 *wapl1-1 wapl2* and *Atsororin wapl1-1 wapl2* mutants. **a** Inactivation of AtSORORIN  
1092 leads to premature loss of centromeric cohesion at the metaphase to anaphase transition  
1093 during meiosis I. Inlays show magnifications of sister centromeric signals during  
1094 metaphase I. Scale bar = 10  $\mu$ m. **b** Magnifications of images depicting metaphase I  
1095 stages for wild type plants, *Atsororin* single mutants and *Atsororin wapl1-1 wapl2* triple  
1096 mutants. Premature splitting of centromeric signals is evident in the absence of  
1097 AtSORORIN. Centromeres are stained in green and DNA is stained in magenta. Scale  
1098 bar = 10 $\mu$ m. **c** Quantification of the number of centromeric signals from metaphase I to  
1099 prophase II stages in wild type plants (n = 73) and *Atsororin* (n = 25), *wapl1-1 wapl2* (n  
1100 = 22) and *Atsororin wapl1-1 wapl2* (n = 33) mutants. **d** Quantification of the number of  
1101 centromeric signals at metaphase II in wild type plants (n = 13) and *Atsororin* (n = 12),  
1102 *wapl1-1 wapl2* (n = 12) and *Atsororin wapl1-1 wapl2* (n = 15) mutants. **e** Quantification  
1103 of the number of centromeric signals in tetrads (balanced: 4 nuclei with 5 centromere  
1104 signals each) in wild type plants (n = 33) and *Atsororin* (n = 25), *wapl1-1 wapl2* (n =  
1105 28) and *Atsororin wapl1-1 wapl2* (n = 18) mutants.

1106 **Figure 7.** Immunolocalization of the axis protein ASY1, the synaptonemal complex  
1107 protein ZYP1 and the cohesin subunit SCC3 in male meiocytes during late zygotene in  
1108 wild type plants and *Atsororin*, *wapl1-1 wapl2* and *Atsororin wapl1-1 wapl2* mutants.

- 1109 Absence of AtSORORIN does not influence their time of deposition or their relative  
1110 localisation on meiotic chromosomes. Scale bar = 10  $\mu$ m.

1111 **Table 1.** *S. pombe* strains and genotypes

Strain number	Genotype
MG1	<i>cen2(D107):kan-ura4+-lacO his7+::lacI-GFP</i>
MG2	<i>cen2(D107):kan-ura4+-lacO his7+::lacI-GFP sor1::kanMX</i>
MG3	<i>cen2(D107):kan-ura4+-lacO his7+::lacI-GFP wpl1::natMX</i>
MG4	<i>cen2(D107):kan-ura4+-lacO his7+::lacI-GFP sor1::kanMX wpl1::natMX</i>
MG5	<i>cen2(D107):kan-ura4+-lacO his7+::lacI-GFP eso1-G799D</i>
MG6	<i>cen2(D107):kan-ura4+-lacO his7+::lacI-GFP sor1::kanMX eso1-G799D</i>
MG7	<i>cen2(D107):kan-ura4+-lacO his7+::lacI-GFP mis4-242</i>
MG8	<i>cen2(D107):kan-ura4+-lacO his7+::lacI-GFP sor1::kanMX mis4-242</i>
MG9	<i>sor1-pk9::kanMX pds5-myc::kanMX</i>
MG10	<i>pds5-myc::kanMX</i>
MG11	<i>sor1-pk9::kanMX</i>
MG12	<i>sor1-pk9::kanMX psm3-GFP::natMX</i>
MG13	<i>sor1-D303A-pk9::kanMX psm3-GFP::natMX</i>
MG14	<i>sor1-GFP::kanMX</i>
MG15	<i>sor1-Flag::kanMX</i>
JG17331	<i>ade6-M216 lys1-37</i>
JG16900	<i>eso1-G799D</i>
JG16897	<i>sor1::kanMX eso1-G799D</i>
JG16904	<i>eso1-G799D sor1::sor1-wt::hphMX</i>
JG16879	<i>eso1-G799D sor1::sor1-F299A::hphMX</i>
JG16881	<i>eso1-G799D sor1::sor1-V302A::hphMX</i>
JG16883	<i>eso1-G799D sor1::sor1-D303A::hphMX</i>
JG16885	<i>eso1-G799D sor1::sor1-Y305A::hphMX</i>
MG13	<i>sor1::TAP::kanMX</i>
MG14	<i>sor1-F299A::TAP::kanMX</i>
MG15	<i>sor1-V302A::TAP::kanMX</i>
MG16	<i>sor1-D303A::TAP::kanMX</i>
MG17	<i>sor1-Y305A::TAP::kanMX</i>

1112 (other auxotrophic markers not scored)

1113 **Table 2.** Primers used in this study

Name	Sequence (5' -> 3')	Utility
35Sp_Fwd	CACTGACGTAAGGGATGACGCAC	PCR for genotyping BASTA gene
Basta_Rev	GAAGTCCAGCTGCCAGAAAC	
WAPL1.1LP	TCCAATTTAGTGAAACGTGGG	PCR for genotyping <i>WAPL1-1</i> T-DNA insertion line
WAPL1.1RP	ACACACTTGATTGAGAACCCG	
WAPL2LP	TCCAGCAAAACAGACAGGAAG	PCR for genotyping <i>WAPL2</i> T-DNA insertion line
WAPL2RP	CTCAAATCTGCGAACGAAGAG	
LBb1.3	ATTTTGCCGATTTGGAAC	T-DNA border primer for T-DNA insertion lines genotyping
Sororin_geno_Fwd	ATTATCGTCTCAAGCTCTCTCG	PCR for amplifying <i>SORORIN</i> gene
Sororin_geno_Rev	GCAGACATACGGCGAGTTAC	
Sororin_sequencing	GCTCTCTCGAGCCTTCTCA	Sanger sequencing of the PCR product of <i>SORORIN</i> gene
Sororin_compl_Fwd	TCGGTCCAAATATATCAACAGC	PCR for genomic AtSORORIN for complementation line
Sororin_compl_Rev	AAATCGCCACTTCTGTACGC	

1114

# Figure 1

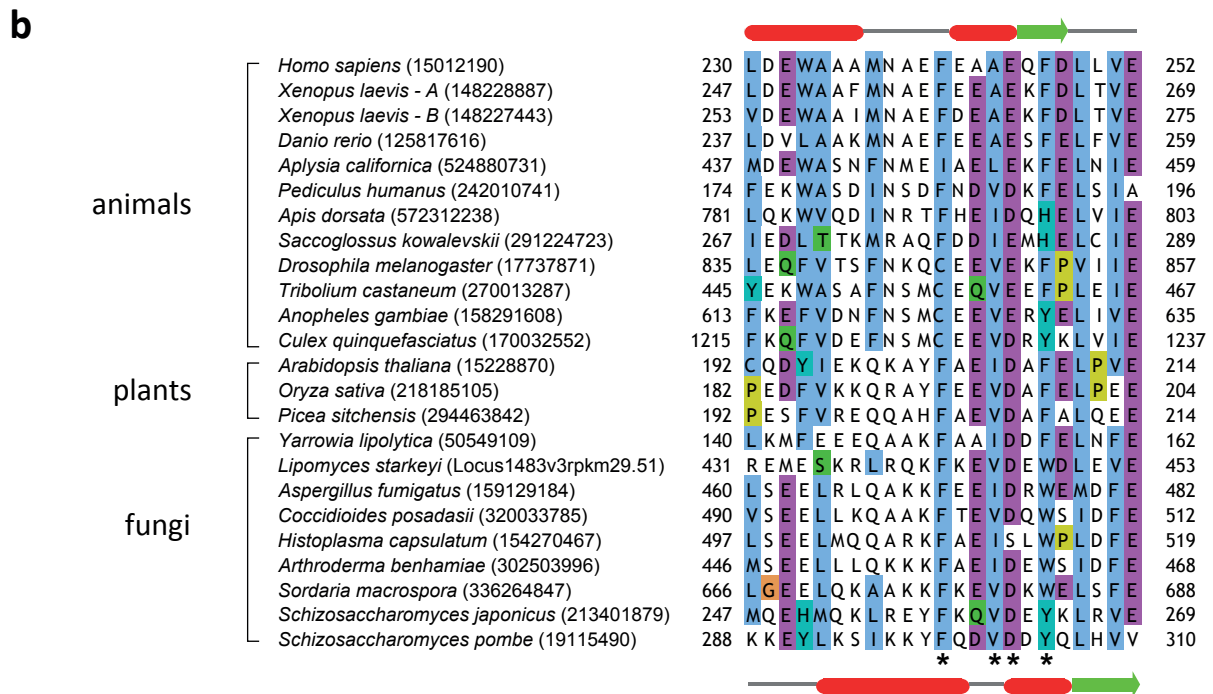
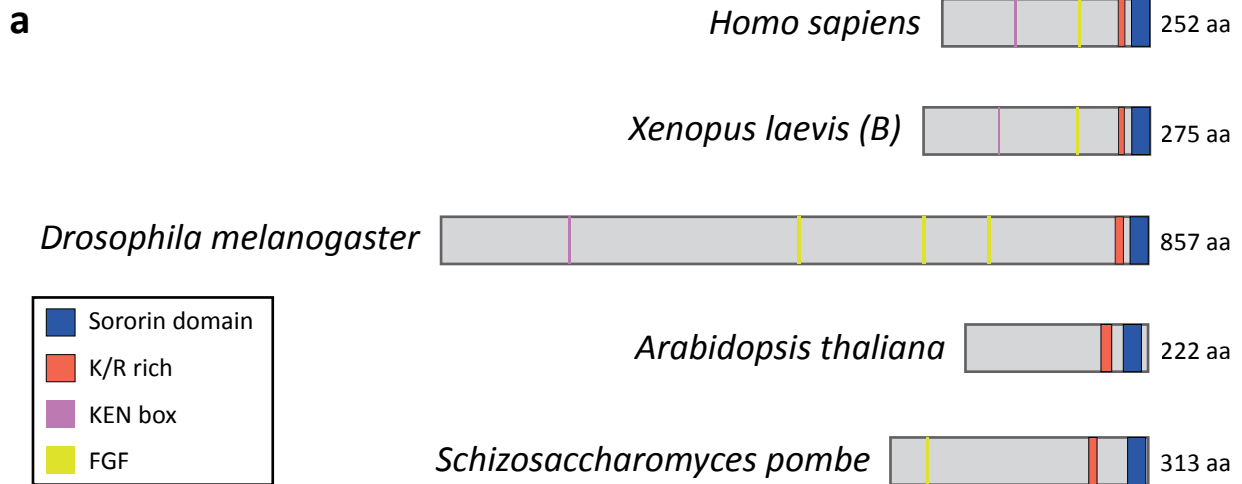


## Figure 2

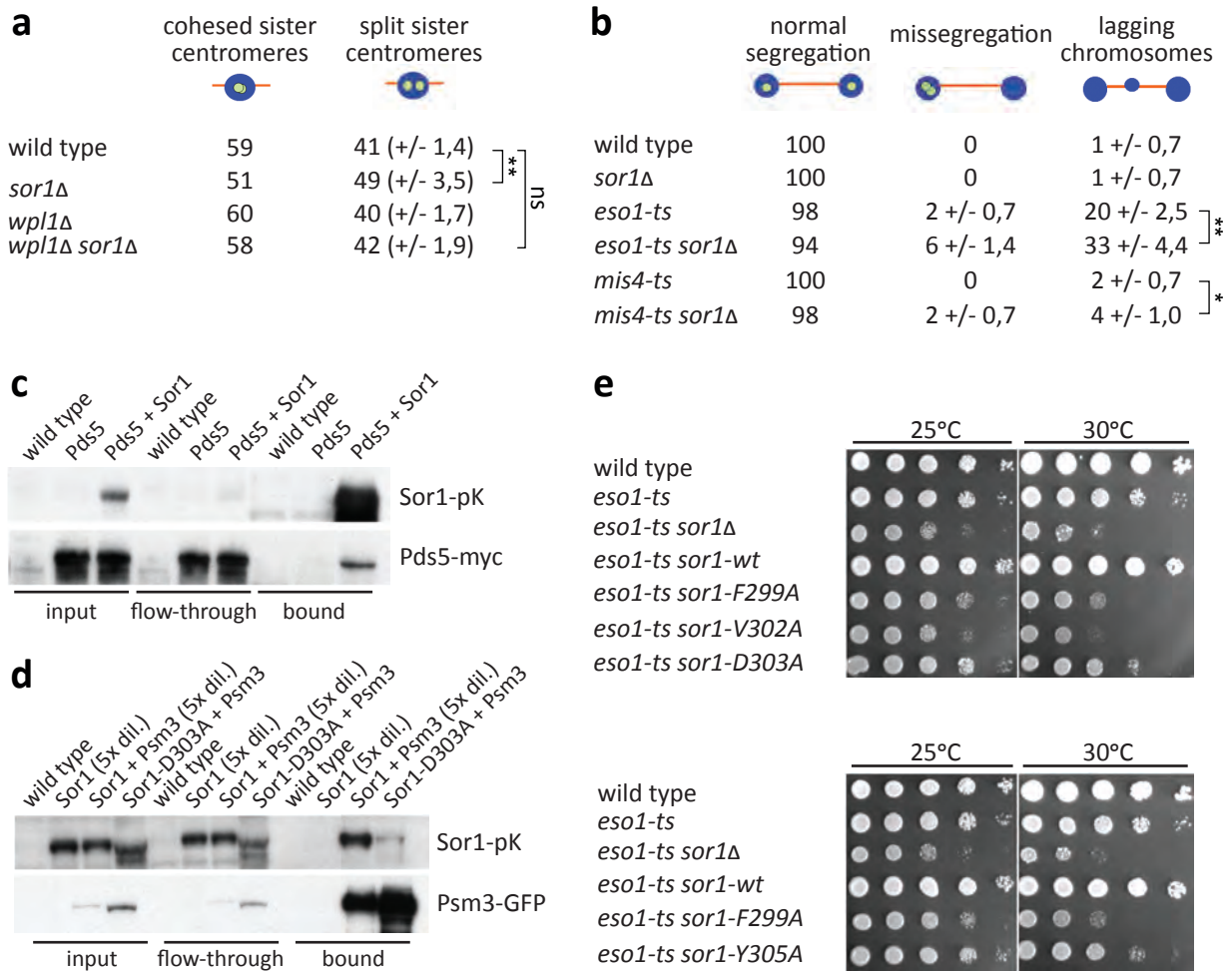




## Figure 3

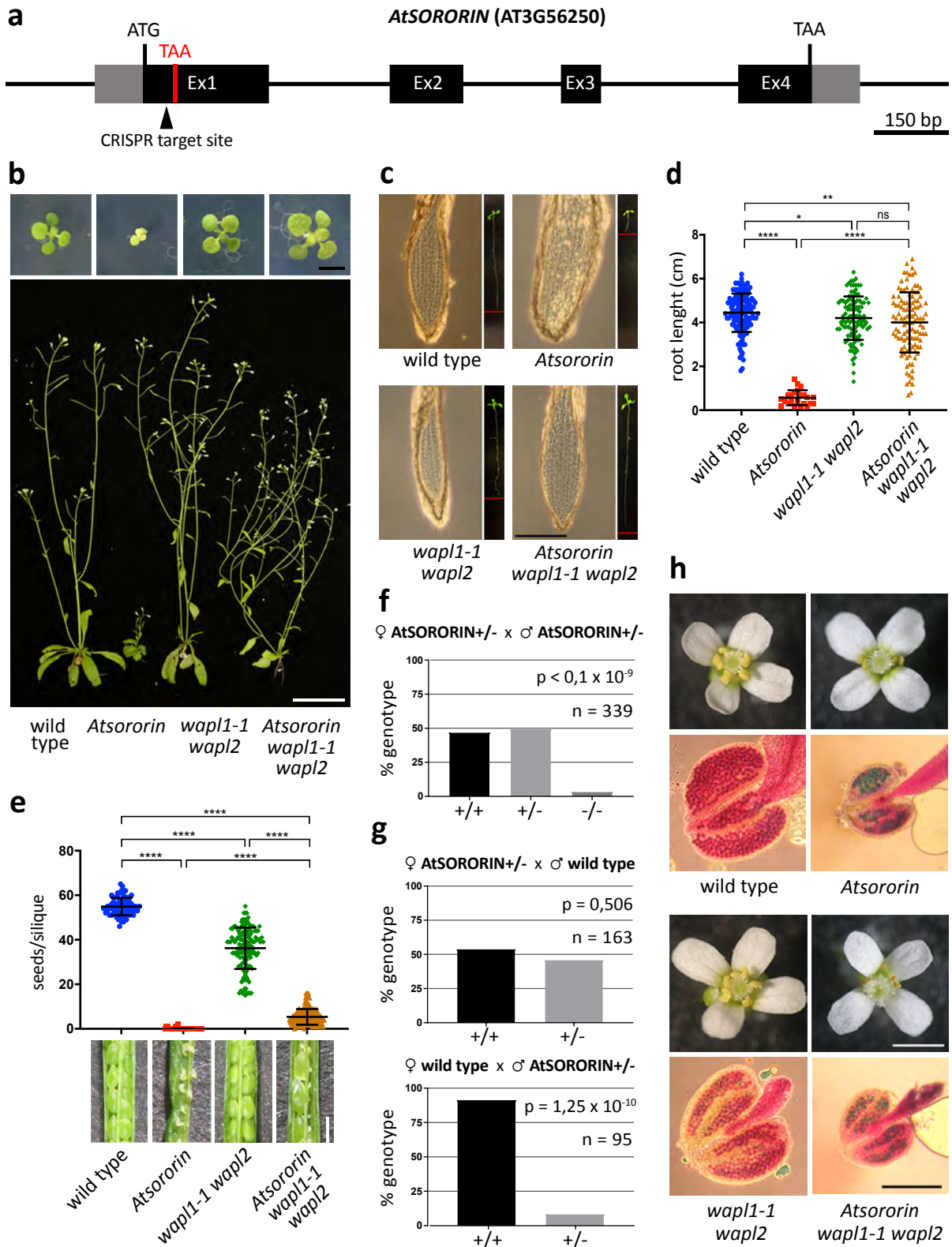


## Figure 4

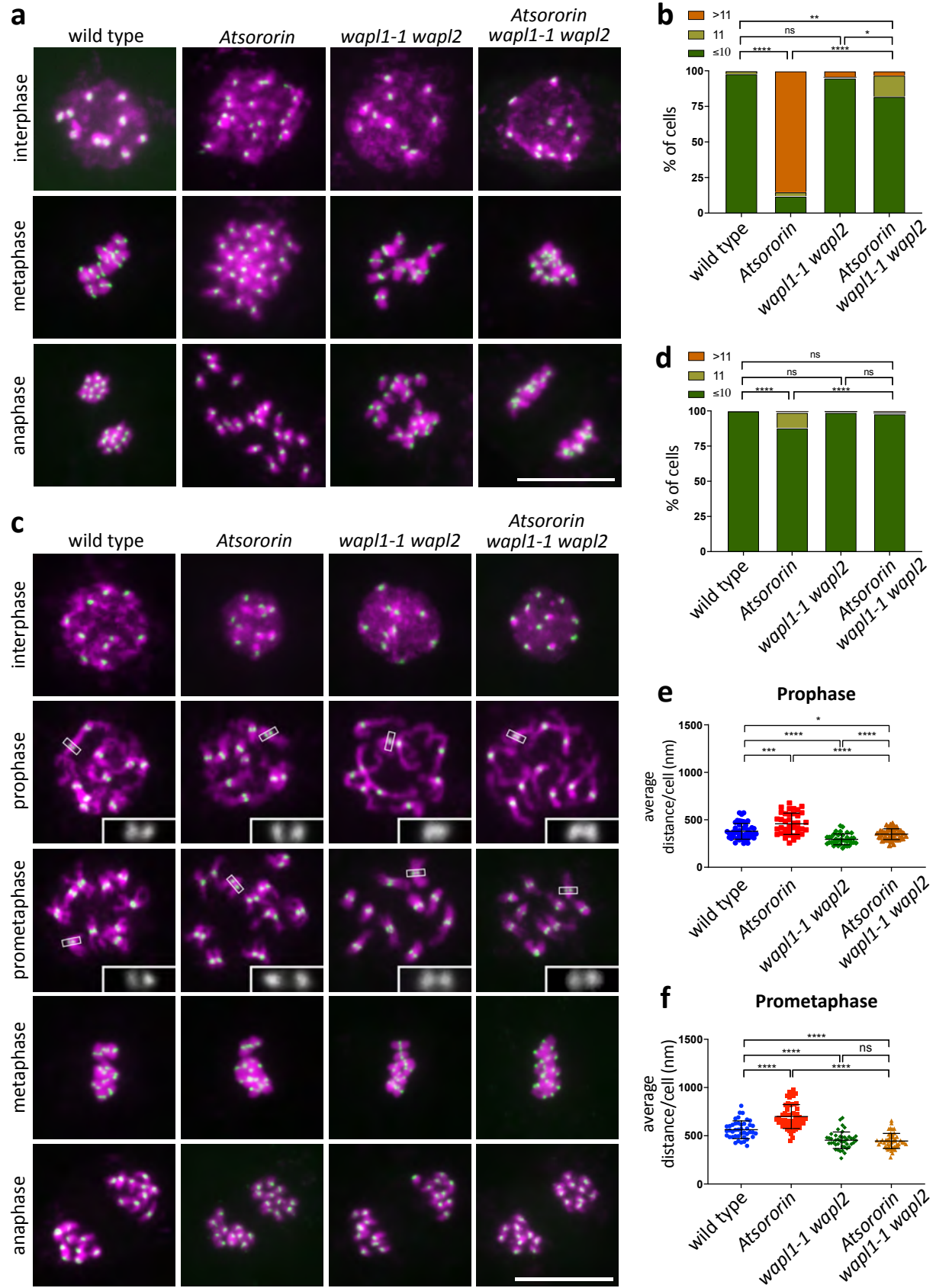


## Figure 5

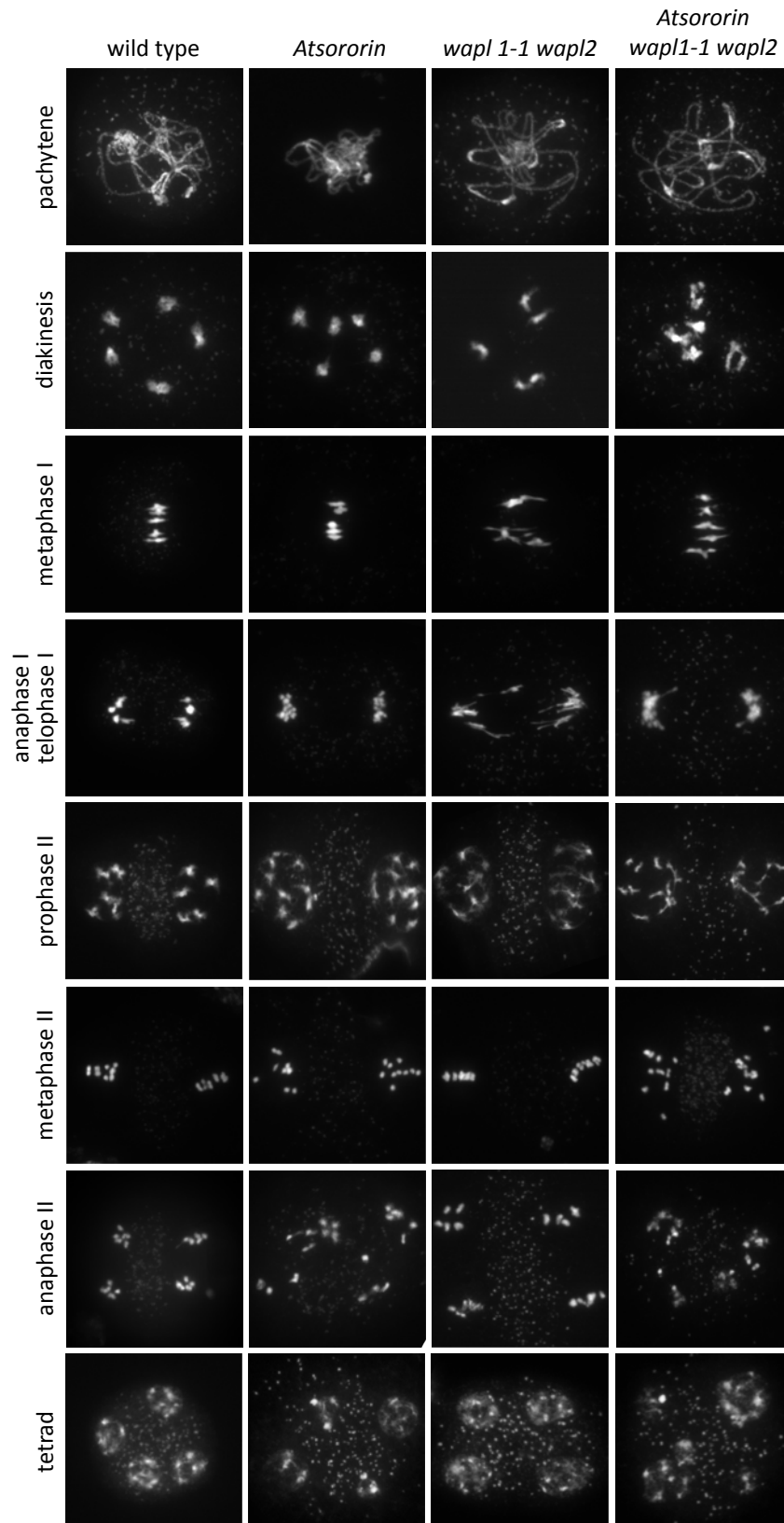
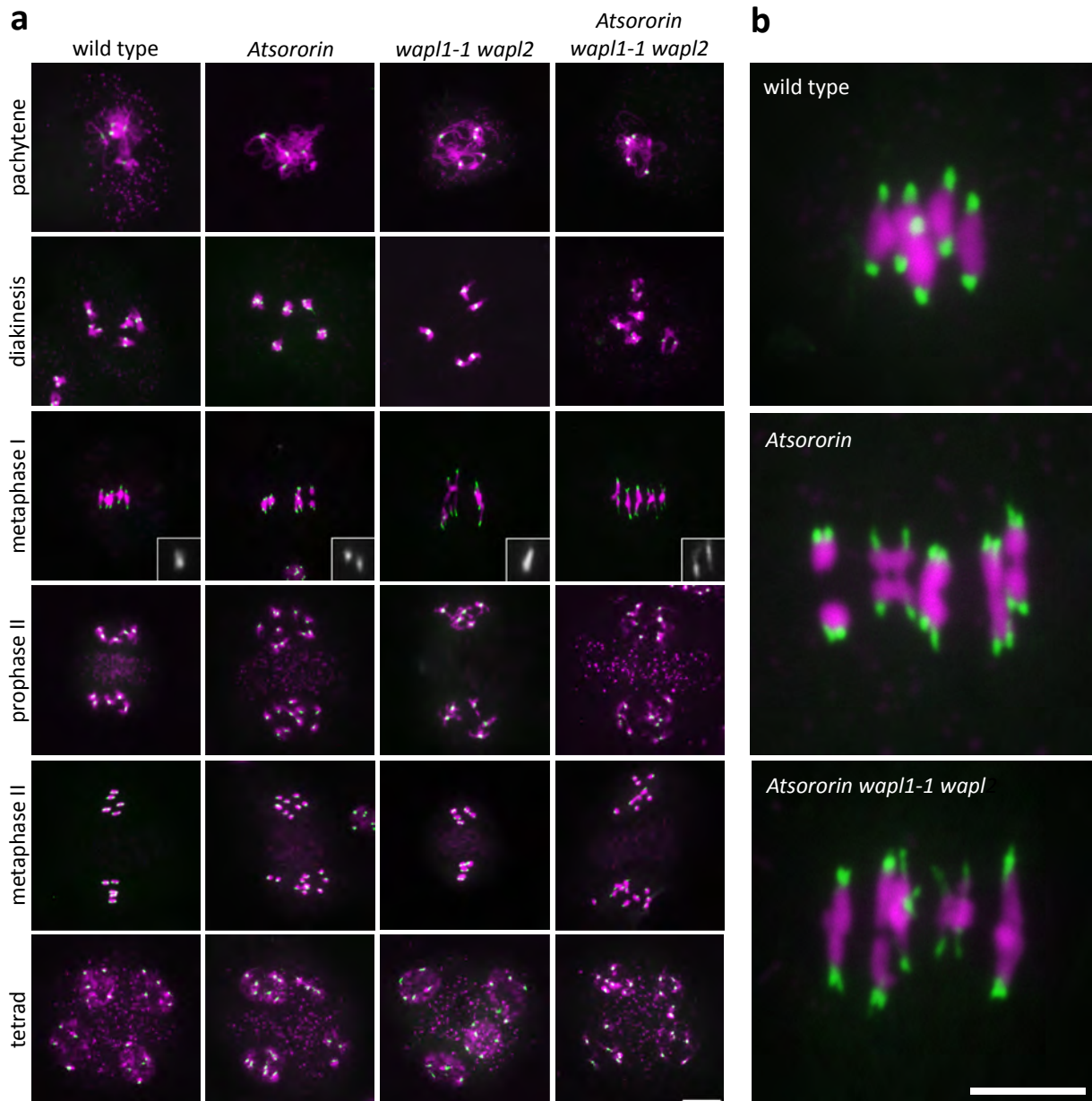
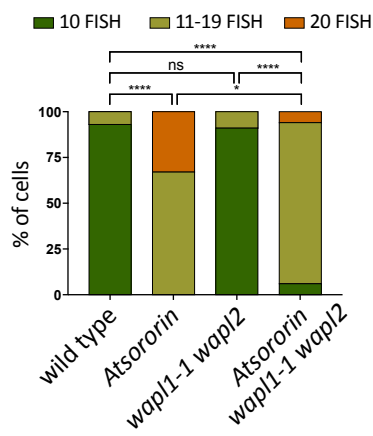


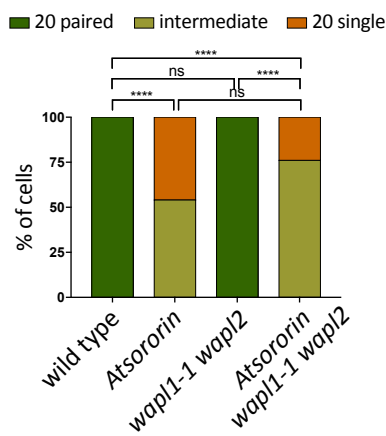
## Figure 6



**c Metaphase I - Prophase II**



**d Metaphase II**



**e Tetrad**

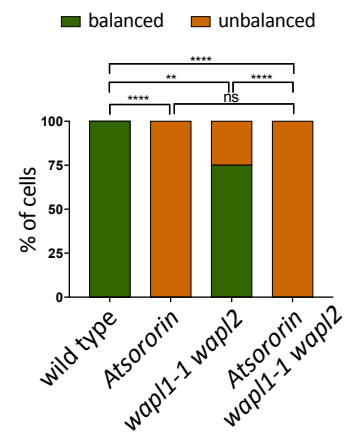
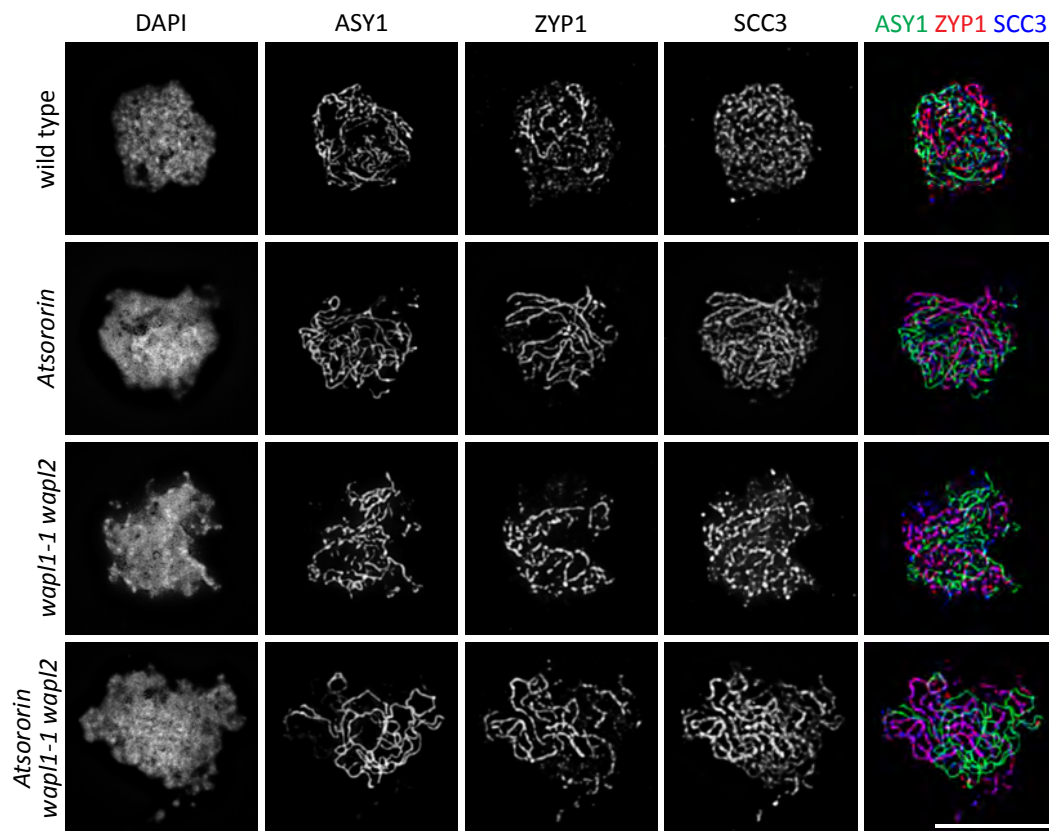


## Figure 7



## **Supplementary information**

**Supplementary Figure 1** (supporting Figure 2). Subcellular localization, APC/C degradation assay and expression analysis of *S. pombe* Sor1. **a, b** Sor1 localizes to nucleus throughout the cell cycle. Cycling *S. pombe* cells expressing Sor1-GFP were fixed, stained with DAPI, and analyzed by fluorescence microscopy (**a**). Cycling *S. pombe* cells expressing Sor1-Flag were fixed and stained with antibodies against Flag and tubulin. Nuclei were visualized by DAPI staining (**b**). **c** *in vitro* assay shows no evidence that Sor1 is an APC/C substrate. **d** Mutating conserved Sor1 residues only slightly reduces Sor1 protein levels. Proteins extracted from cycling cells were analyzed by gel electrophoresis and Western blotting using anti-tubulin antibodies. The TAP epitope was detected using PAP antibodies (rabbit antiperoxidase antibody linked to peroxidase).

**Supplementary Figure 2** (supporting Figures 3 and 4). Meiotic and somatic *Atsororin* mutant phenotypes can be complemented with the wild type *AtSORORIN* gene. **a** Overall plant architecture and fertility are wild type-like in the complemented transgenic plant line, but not in the *Atsororin* mutant. **b** Seed counts demonstrate nearly wild type-like fertility of the complemented transgenic plant line, but sterility in the *Atsororin* mutant. Unpaired Mann-Whitney test has been applied (\*\*\*\* $p < 0.0001$ ). Somatic defects in *Atsororin* mutants are tissue-specific and WAPL-dependent. DNA was stained with DAPI (magenta) and fluorescence *in situ* hybridization (FISH) was performed to detect centromeric regions (green). **c** Spreads of cell nuclei from rosette leaf cells. Interphase stages were analyzed for wild type plants and *Atsororin*, *wapl1-1 wapl2* and *Atsororin wapl1-1 wapl2* mutants. The number of centromeric signals is indicated in the top left corner. Scale bar = 10 $\mu$ m. **d** Quantification of centromeric-FISH signals in interphase leaf nuclei. *Atsororin* mutants (n = 52) have a significantly higher number of cells that have more than 10 signals, when compared to wild type (n = 84), *wapl1-1 wapl2* (n = 68) and *Atsororin wapl1-1 wapl2* (n = 82). Chi-square test was performed (\*\*\*\* $p < 0.0001$ ).

**Supplementary Figure 3** (supporting Figure 7). Immunolocalization of the axis protein ASY1 and the meiosis-specific cohesin subunit REC8 in male meiocytes during late zygotene in wild type plants and *Atsororin*, *wapl1-1 wapl2* and *Atsororin wapl1-1 wapl2* mutants. Absence of *AtSORORIN* does not influence their time of deposition or their relative localisation on meiotic chromosomes. Scale bar = 10  $\mu$ m.

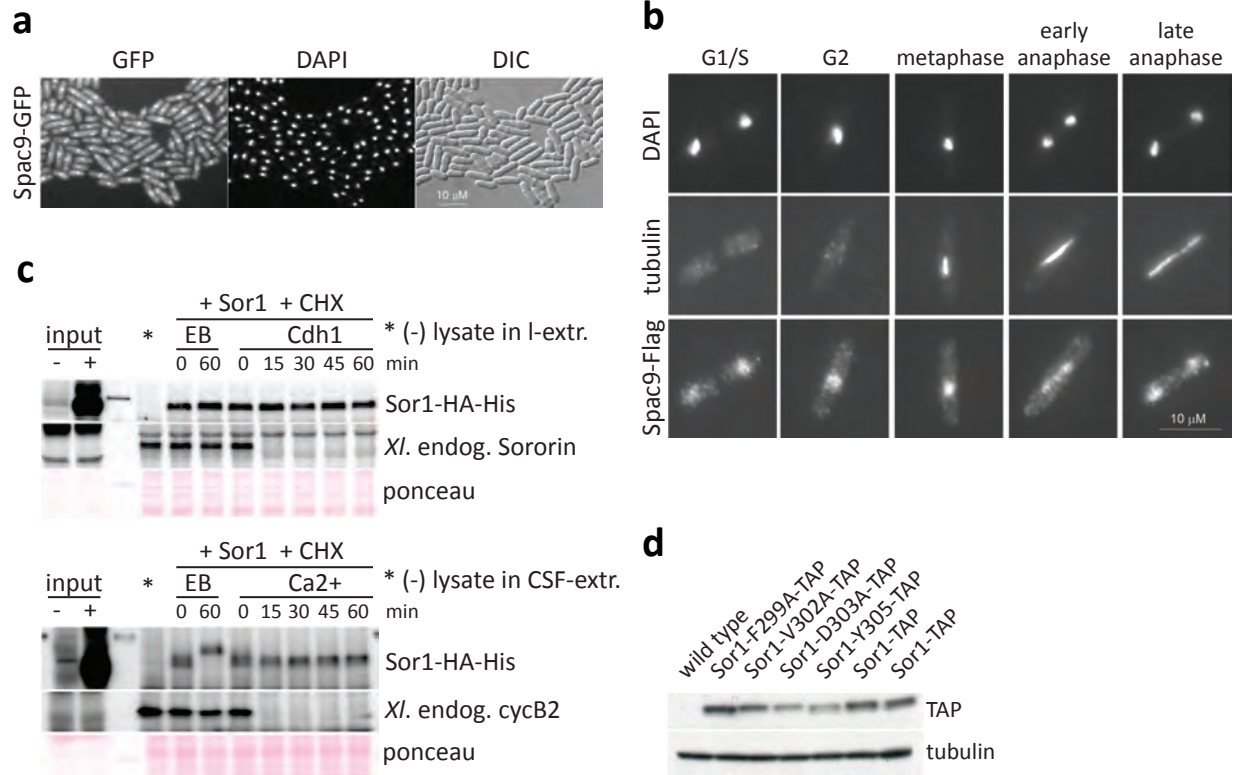
**Supplementary Movie 1.** Root tips from wild type plants display normal tissue organization and nucleus size.

**Supplementary Movie 2.** Root cellular organization and nucleus size are highly affected in *Atsororin* mutant plants.

**Supplementary Movie 3.** Plants with mutations in both genes encoding WAPL (*wapl1-1 wapl2*) develop normal roots compared to wild type plants.

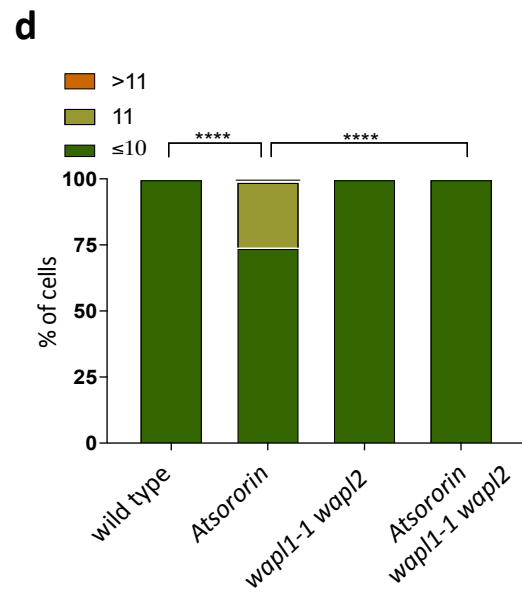
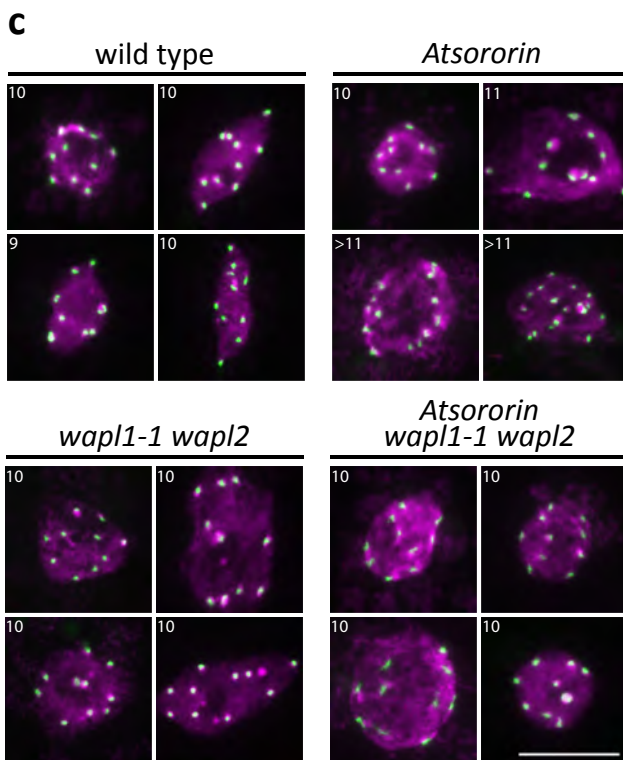
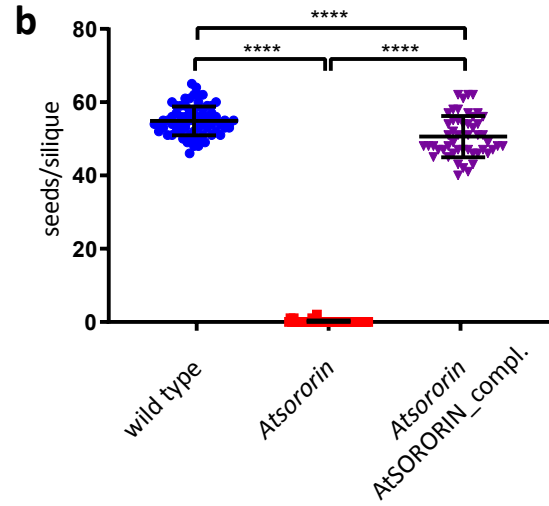
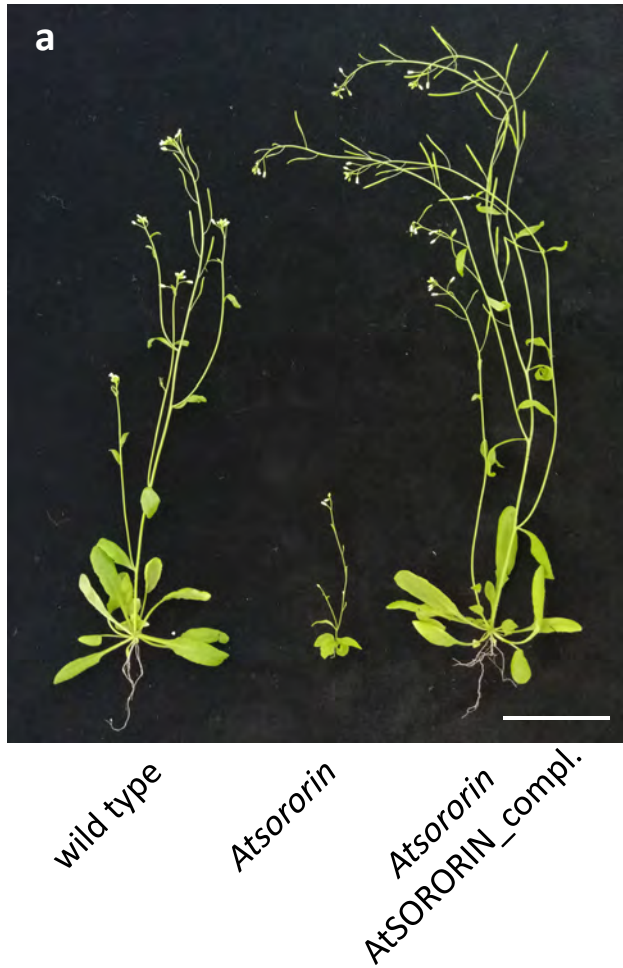
**Supplementary Movie 4.** *Atsororin wapl1-1 wapl2 triple* mutant plants develop normal roots, indicating that the *wapl1-1 wapl2* mutations suppress the effect of the *Atsororin* mutation with respect to root development.

# Supplementary Figure 1





## Supplementary Figure 2



## Supplementary Figure 3

